Mechanistic Insight Into the Photoredox Catalysis of Anti-Markovnikov Alkene Hydrofunctionalization Reactions

Nathan A. Romero and David A. Nicewicz*

Department of Chemistry, University of North Carolina at Chapel Hill, New Venable Laboratories, Chapel Hill, NC 27599-3290, USA

E-mail:nicewicz@unc.edu

Table of Contents

I. General Information

General Methods. All synthetic manipulations were carried out as reported by our laboratory previously,[1] using air-free techniques when appropriate. The purity of all synthesized materials was verified by ^{1}H NMR to be >97% (Bruker model DRX-400, 500, or 600 spectrometer). Chemical shifts are referenced to residual $CHCl_3$ (7.26 ppm) in the solvent for proton signals and to the carbon resonance (77.16 ppm) of the solvent for ^{13}C signals as parts per million downfield from tetramethylsilane. Unless otherwise noted, all solutions used in spectroscopic measurements were prepared in a dry, nitrogen filled glovebox in which O_2 levels were kept below 2.0 ppm at all times. Preparative photolysis experiments utilized a single Par38 Royal Blue Aquarium LED lamp (Model # 6851) fabricated with high-power Cree LEDs as purchased from Ecoxotic (www.ecoxotic.com). For all photolyses, reactions were stirred using a PTFE coated magnetic stir bar on a magnetic stir plate. The lamp was positioned approximately 10 cm from the reaction vial.

Materials. Spectrophotometric grade acetonitrile (MeCN) and 1,2-dichloroethane (DCE) were purchased from EMD Millipore and were distilled from P_2O_5, sparged with dry Nitrogen or Argon gas for at least 1 hour, and immediately transferred to the glovebox. Solid samples were purified by recrystallization unless otherwise specified. Authentic 9-mesityl-10-methylacridinium tetrafluoroborate (Mes-AcrBF$_4$) was synthesized as reported previously,[2] and highly pure samples were obtained after three successive recrystallizations using an acetonitrile/methanol mixture (MeCN/MeOH = ~5:1) to dissolve the acridinium at room temperature, followed by careful layering with an equal volume of diethyl ether (Et_2O). After an initial period of crystallization, an excess of Et_2O was further layered in order to promote additional crystallization. The solid was collected by vacuum filtration and dried under vacuum for 24 hours. Bis(η^5-cyclopentadienyl)cobalt (cobaltocene = **CoCp$_2$**) was purchased from Strem and used without further purification. Diphenyl disulfide (**PhS**)$_2$ was recrystallized from ethanol/hexanes and dried under vacuum for 24 hours for all studies except crossover experiments. In crossover studies, diphenyl disulfide (**PhS**)$_2$ and di-*p*-tolyl disulfide (**4-Me-PhS**)$_2$ were used as received from Sigma-Aldrich (>98% pure). Thiophenol (**PhSH**), Anethole ((*E*)-1-methoxy-4-(prop-1-en-1-yl)benzene, **An**) and β-methylstyrene ((*E*)-prop-1-en-1-ylbenzene, **βMS**) were purchased from Sigma-Aldrich and purified by distillation. Other materials used in Stern-Volmer experiments (5-methyl-2,2-diphenylhex-4-enoic acid, 5-methyl-2,2-diphenylhex-4-en-1-ol, 2-phenylmalononitrile (**PMN**)) were authentic samples used in a previous report from our laboratory.[1]

Synthesized Materials:

9-Xylyl-10-methylacridinium tetrafluoroborate (Xyl-AcrBF$_4$) was synthesized according to the previously specified method for 9-mesityl-10-methylacridinium tetrafluoroborate,[2] with 2-bromo-1,3-dimethylbenzene used in place of 2-bromo-1,3,5-trimethylbenzene. **Xyl-**

Acr$^+$ was recrystallized from MeCN/MeOH in the same way as **Mes-Acr$^+$.** The ^{1}H and ^{13}C NMR chemical shifts are consistent with those reported for the iodide salt in DMSO-d_6.[3]

^{1}H NMR (600 MHz, Chloroform-*d*) δ 8.84 (dd, *J* = 9.4, 2.2 Hz, 2H), 8.46 – 8.40 (m, 2H), 7.84 – 7.77 (m, 4H), 7.51 (t, *J* = 7.8 Hz, 1H), 7.34 (d, *J* = 7.7 Hz, 2H), 5.11 (s, 3H), 1.76 (s, 6H). ^{13}C NMR (151 MHz, $CDCl_3$) δ 162.14, 141.78, 139.62, 136.19, 132.47, 130.45, 128.79, 128.64, 128.43, 125.80, 119.63, 39.28, 20.27.

(*E*)-5-Phenylpent-4-en-1-ol (R-OH) was synthesized from benzaldehyde according to the procedure reported previously for the synthesis of 5-aryl-2,2-dimethylpent-4-en-1-ols.[1] The ^{1}H NMR chemical shifts match those reported in the literature.[4]

^{1}H NMR (500 MHz, Chloroform-*d*) δ 7.39 – 7.35 (m, 2H), 7.32 (dd, *J* = 8.6, 6.8 Hz, 2H), 7.23 (t, *J* = 7.3 Hz, 1H), 6.45 (d, *J* = 15.8 Hz, 1H), 6.26 (dt, *J* = 15.8, 6.9 Hz, 1H), 3.74 (t, *J* = 6.4 Hz, 2H), 2.34 (q, *J* = 7.2Hz, 2H), 1.79 (p, *J* = 6.9 Hz, 2H), 1.32 (t, *J* = 4.6 Hz, 1H).

***Tert*-Butyldimethyl-(*E*)-(5-phenylpent-4-enyloxy)silane (R-OTBDMS)** was synthesized from the corresponding alkenol as reported previously,[4] and the ^{1}H NMR matches the reported chemical shifts.[4]

^{1}H NMR (600 MHz, Chloroform-*d*) δ 7.35 (d, *J* = 7.0 Hz, 2H), 7.30 (t, *J* = 7.6 Hz, 2H), 7.21 (t, *J* = 7.3 Hz, 1H), 6.41 (d, *J* = 15.8 Hz, 1H), 6.25 (dt, *J* = 15.8, 6.9 Hz, 1H), 3.68 (t, *J* = 6.4 Hz, 2H), 2.29 (q, *J* = 6.9 Hz, 2H), 1.72 (p, *J* = 6.3 Hz, 2H), 0.93 (s, 9H), 0.08 (s, 6H).

10-Methylacridinium tetrafluoroborate ($AcrBF_4$) was synthesized by addition of acridine to trimethyloxonium tetrafluoroborate (Me_3OBF_4) in DCE. The salt was precipitated with Et_2O and recrystallized repeatedly from MeCN/MeOH and Et_2O. The ^{1}H NMR is consistent with the literature report in DMSO-d_6.[5]

^{1}H NMR (400 MHz, Chloroform-*d*) δ 8.95 (d, *J* = 8.3 Hz, 2H), 8.22 – 8.14 (m, 2H), 8.07 (d, *J* = 9.0 Hz, 2H), 7.92 (br s, 1H), 7.73 (t, *J* = 7.7 Hz, 2H), 4.47 (s, 3H).

10-Methylacridinium Chloride (AcrCl) was employed in the determination of fluorescence quantum yield of **Mes-AcrBF$_4$**. **AcrCl** was obtained by dissolving **AcrBF$_4$** in concentrated aqueous HCl, and crystals were collected after addition of ethanol/diethyl ether (1:1). After recrystallizing twice from ethanol, analytically pure material was used in subsequent photophysical studies. The absolute fluorescence quantum yield of **AcrCl** in H_2O is widely accepted to be 1.0,[6] and the quantum yield of **Mes-AcrBF$_4$** in DCE reported herein is measured relative to the quantum yield of **AcrCl**.

^{1}H NMR and ^{13}C NMR spectra for Xyl-AcrBF$_4$ (CDCl$_3$):

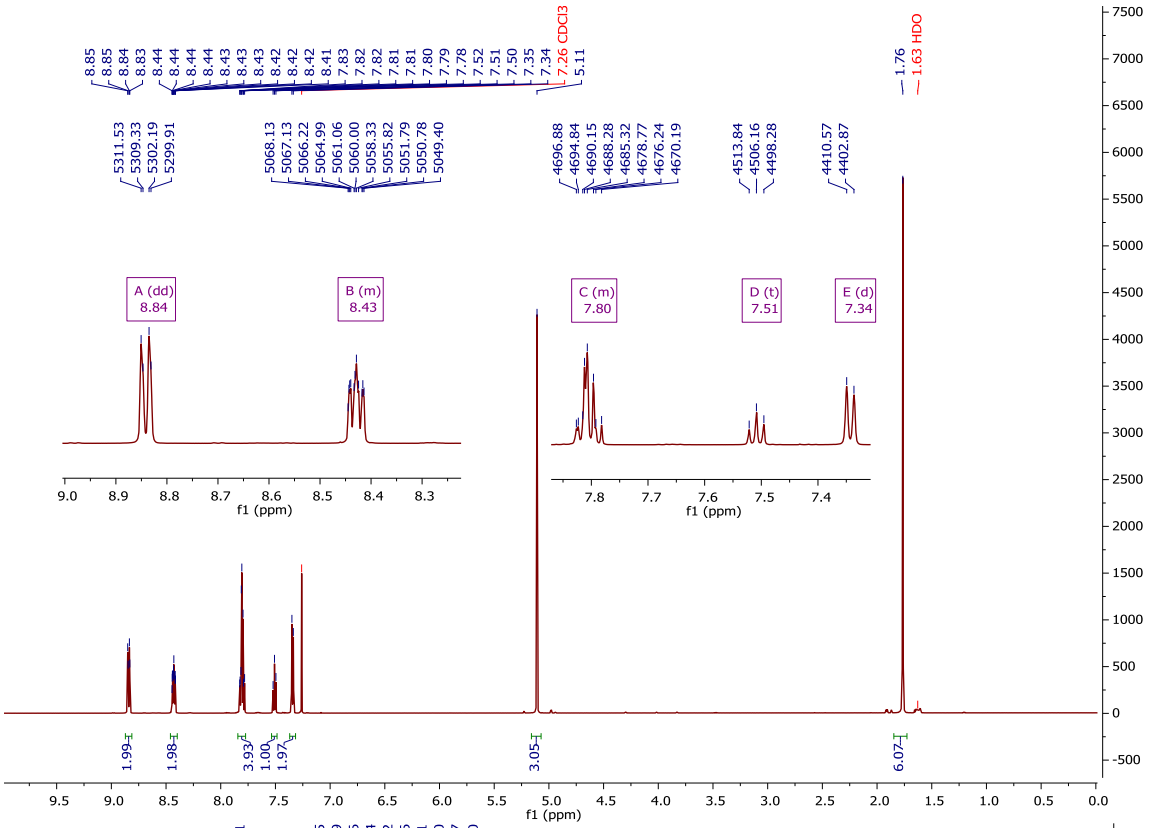

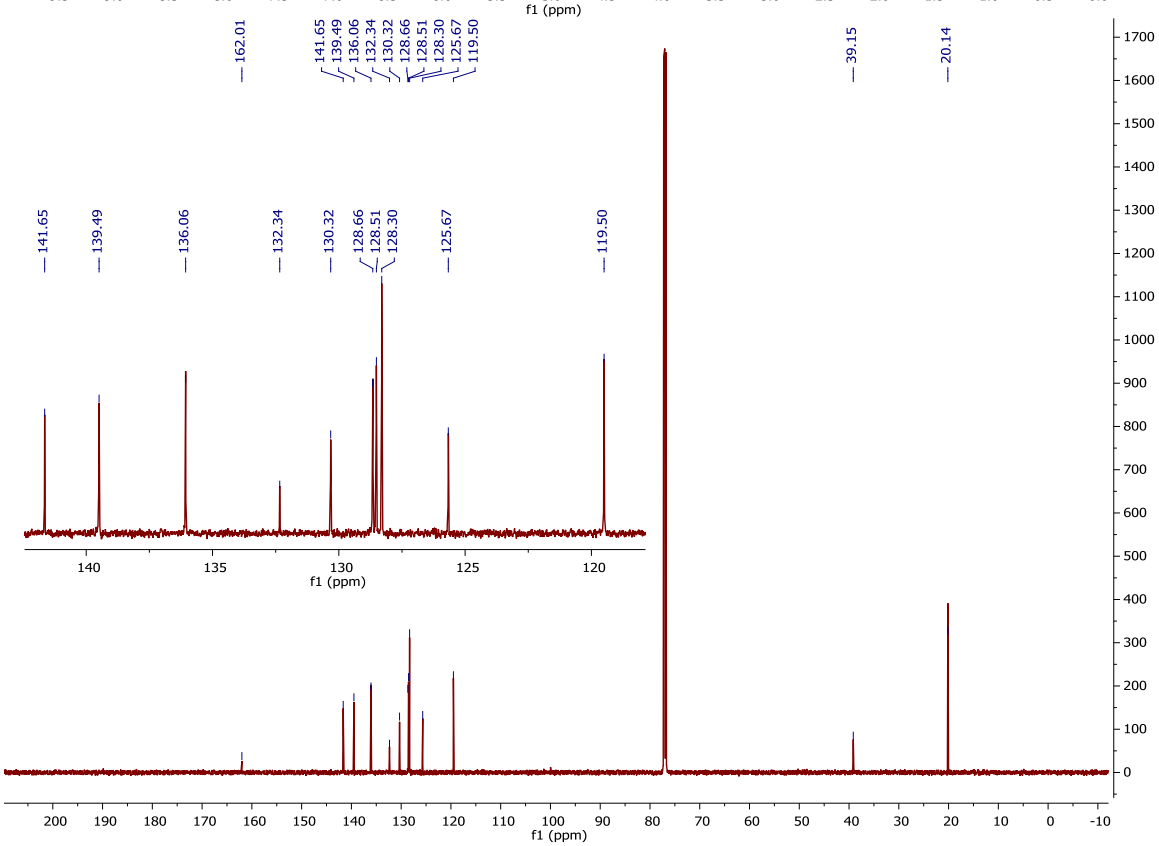

II. Spectroelectrochemical Measurements

Spectroelectrochemical measurements were performed in a N_2 filled glovebox with the use of a Pine Instruments honeycomb spectroelectrochemical cell in combination with the Wavenow potentiostat from the same manufacturer. Absorption spectra were collected using an Agilent Cary 60 spectrophotometer equipped with optical fiber manufactured by Ocean Optics. The spectrum for neutral **Mes-Acr•** was recorded by performing bulk electrolysis on a solution of Mes-AcrBF$_4$ (93 µM) in DCE with 0.1 M tetrabutylammonium tetrafluoroborate (TBABF$_4$) as a supporting electrolyte. When the potential was fixed at -1.0 V (nominal) using a platinum working electrode, complete conversion of **Mes-Acr**$^+$ to **Mes-Acr•** occurred within 30 seconds. The absorbance spectrum of **Mes-Acr•** at complete conversion was converted to molar absorptivity (ε) using a reference value of 6340 $M^{-1}cm^{-1}$ at 430 nm for **Mes-Acr**$^+$ in DCE. The calculated molar absorptivity at 520 nm is 6610 $M^{-1}cm^{-1}$. The difference spectrum for **Mes-Acr•** (Figure S10, red) was obtained by subtraction of the absorption spectrum prior to electrolysis from the spectrum after complete conversion to **Mes-Acr•**.

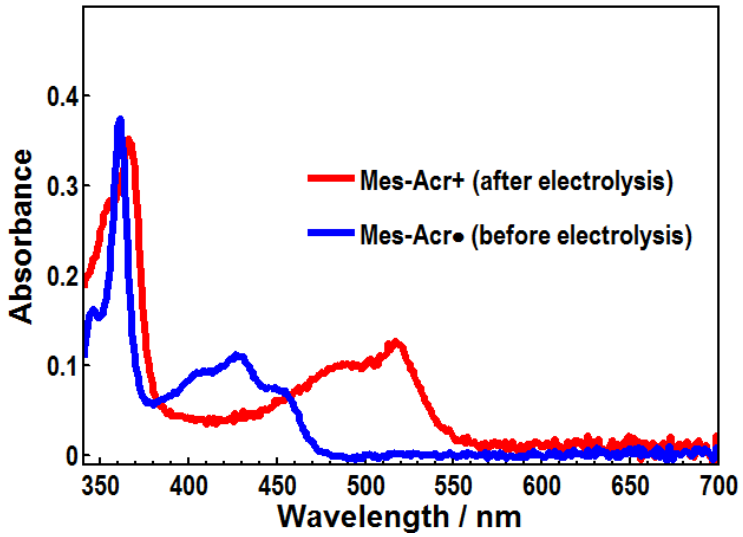

Figure S1. UV-Vis absorbance spectra collected before (red) and after (blue) bulk electrolysis at a fixed potential of -1.0 V (nominal) on a 93 µM solution of Mes-AcrBF$_4$ in DCE with 0.1 M TBABF$_4$ as a supporting electrolyte.

III. Electrochemical Measurements

Cyclic Voltammetry was performed using a Pine Instruments Wavenow potentiostat with a standard three electrode setup (working: glassy carbon, reference: Ag/AgCl in 3 M NaCl, counter: platinum). All measurements were taken in N_2-sparged MeCN with 0.1 M tetrabutylammonium hexafluorophosphate (TBAPF$_6$) as a supporting electrolyte where the analyte concentration was 5-10 mM. The potential was scanned from 1.0 V to a vertex potential

of 2.5 V in the forward direction at a sweep rate of 100 mV/s, and the reverse sweep showed no indication of a reversible electrochemical event in all cases. The voltammograms shown below have been corrected by subtracting the background current of the electrolyte solution. The half-wave potential for irreversible oxidation is estimated at $E_{p/2}$ the potential where the current is equal to one-half the peak current of the oxidation event. The values for $E_{p/2}$ are referenced to SCE (Saturated Calomel Electrode) by adding $^{+}$30 mV to the potential measured against Ag/AgCl (3 M NaCl).

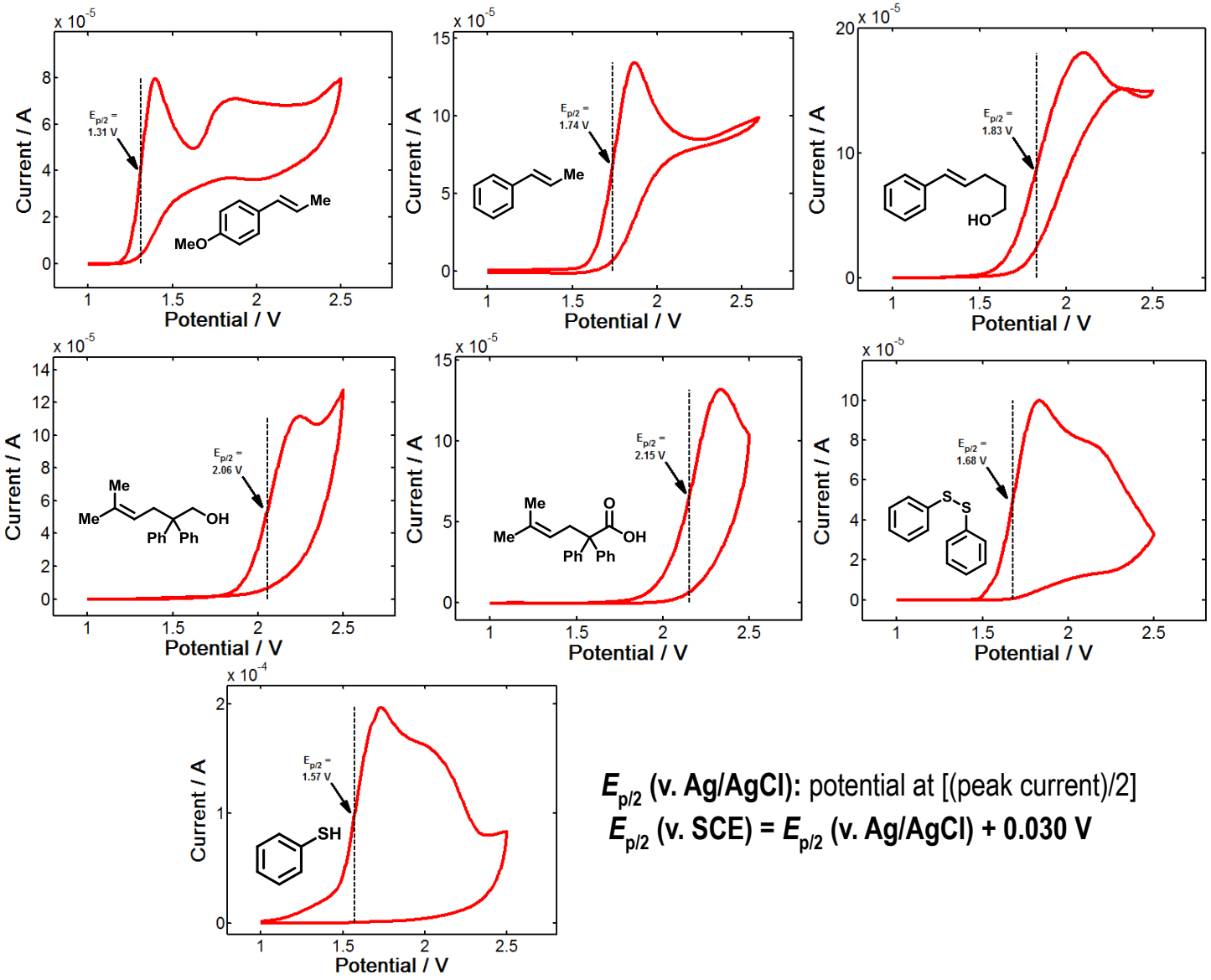

$E_{p/2}$ (v. Ag/AgCl): potential at [(peak current)/2]

$E_{p/2}$ (v. SCE) = $E_{p/2}$ (v. Ag/AgCl) + 0.030 V

Figure S2. Cyclic voltammograms for the species examined in this study. The $E_{p/2}$ values shown on each plot referenced to Ag/AgCl in 3 M NaCl. Addition of 30 mV to this value gives the potential v. SCE.

IV. Photophysical Measurements: General Information.

All photophysical measurements were taken in 4 ml (nominal volume) quartz cells sealed with a silicone rubber- or PTFE-lined screw cap purchased from Starna Cells, Inc. Solutions were made by dilution and thorough mixing of freshly prepared stock solutions of each component to a total volume of 4.0 mL unless otherwise stated. Background absorbance of the solvent is subtracted from the reported spectra. Duplicate experiments were performed to ensure the reproducibility of all results, and the reported data is the composite of all trials. In most cases, error is estimated from multiple trials and is represented as the maximum deviation from the average of multiple measurements.

Prior to laser flash photolysis or fluorescence experiments, each sample was evaluated by UV-Vis absorption to verify **Mes-Acr**$^+$ concentration. Where relevant, UV-Vis absorption spectra were measured during or after analysis to determine sample degradation. Steady state UV-Vis absorption spectra were recorded on a Varian Cary 50 spectrophotometer or a Hewlett-Packard 8453 Chemstation spectrophotometer. Molar extinction coefficients for Mes-AcrBF$_4$ in DCE were determined by concentration studies (ε = 6340 $M^{-1}cm^{-1}$ at 430 nm), and all subsequent optical measurements employed sample concentrations in the region where the detector response was found to be linear with respect to absorbance at 430 nm.

V. Emission Studies

Time-resolved and steady state emission spectra were recorded using an Edinburgh FLS920 spectrometer. The temperature of the cell was controlled with a Quantum Northwest TLC 50 4-position cell holder where the temperature was modulated by a Peltier device. Unless otherwise specified, measurements were taken under ambient conditions. Each sample was stirred continuously with a magnetic stir bar. For collection of steady state fluorescence spectra, the excitation wavelength was set to 450 nm, and a 435 nm low pass optical filter was used to remove extraneous wavelengths from the excitation light. All spectra (1 nm step size, 5 nm bandwidth) are fully corrected for the spectral response of the instrument. Time resolved emission measurements (including Stern-Volmer quenching studies) were made by the time-correlate single photon counting (TCSPC) capability of the same instrument (FLS920) with pulsed excitation light (444.2 nm, typical pulse width = 95 ps) generated by a Edinburgh EPL-445 ps pulsed laser diode operating at a repetition rate of 5 MHz for **Mes-Acr**$^+$ or 2 MHz for **Xyl-Acr**$^+$ and **Acr**$^+$. The maximum emission channel count rate was less than 5% of the laser channel count rate, and each data set collected greater than 7500 counts on the maximum channel. The fluorescence lifetime of Mes-AcrBF$_4$ was found not to depend on stirring, exposure to air, or repetition rate of the laser diode with detection at 500 or 515 nm (20 nm bandwidth). The lifetime of fluorescence was determined by reconvolution fit with the instrument response function using the Edinburgh FS900 software. In all cases, after reconvolution, fluorescence decay was satisfactorily fit with a monoexponential function of the form:

$$I_t = I_0 e^{-t/\tau} \quad \text{(eq. S1)}$$

where I is the intensity (counts), and τ is the mean lifetime of fluorescence. Fluorescence lifetimes for **Mes-Acr**$^+$, **Xyl-Acr**$^+$, and **Acr**$^+$ were measured with detection at 500 nm with solutions in 4.0 mL DCE at concentrations of 1.60×10^{-5} M in each. Repetition rate was 5 MHz for **Mes-Acr**$^+$ and 2 MHz for **Xyl-Acr**$^+$ and **Acr**$^+$.

NOTE: While both LE^S and CT^S (for **Mes-Acr**$^+$) are reported to decay with a common lifetime of ~6 ns, we observe minor differences in the fluorescence lifetimes when the time resolved emission spectra are measured with the LP920 instrument (Figure S4, see **Section VII** below). Though CT^S appears to decay slightly faster than LE^S (Figure S4), the difference is evidently minimal at 500 and 515 nm, such that the fluorescence decay at these wavelengths follows single exponential kinetics when measured by TCSPC. Nonetheless, we use this difference in fluorescence lifetime to approximate the contribution of CT^S to the steady state fluorescence. The red trace in Figure S3 below is produced by normalizing the raw transient emission spectra at 20 ns and 60 ns at to 475 nm, and subtracting the spectrum at 60 ns from the spectrum at 20 ns. Thus, at 60 ns, the emission is almost entirely due LE fluorescence.

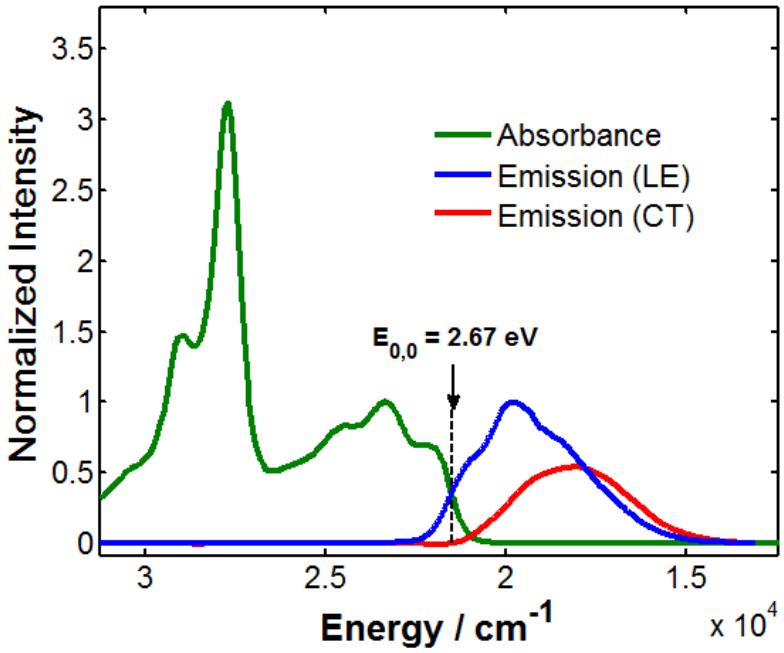

Figure S3. Steady state absorbance spectrum (red, measured on HP 8453 spectrophotometer) and emission spectra for **Mes-Acr**$^+$ (measured on LP920) where locally excited (LE, blue) and charge-transfer (CT, red) fluorescence contributions are separated. Excitation energy $E_{0,0}$ is determined to be 2.67 eV at the intersection of absorption and LE fluorescence spectra normalized to 1. The calculated $E_{0,0}$ is identical to the value obtained by Verhoeven, et. al.[7] Accordingly, the excited state reduction potential is calculated to be +2.12 V vs. SCE (E^*_{red} = $E_{0,0}$ + E_{red} = (2.67 – 0.55) V = +2.12 V).

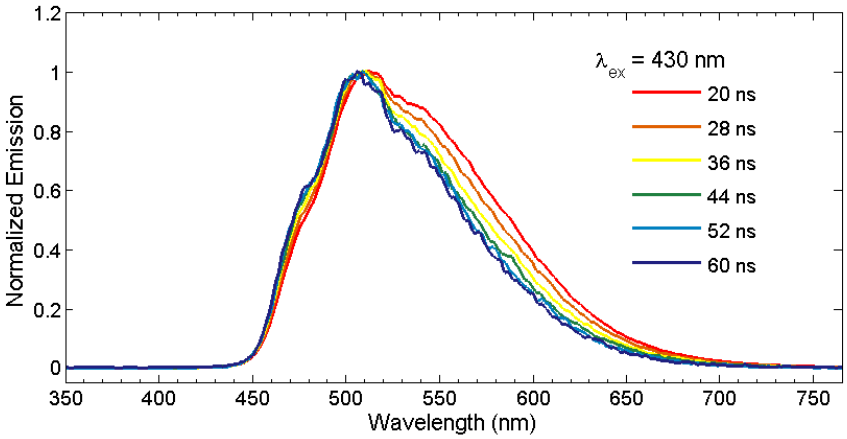

Figure S4. Time resolved emission spectra for **Mes-Acr**$^{+}$ (50 µM, measured on LP920) normalized at 510 nm to show both LE and CT. Contribution of CT^{S} fluorescence (Figure S3) estimated by subtracting the emission spectrum at 60 ns from the emission spectrum at 20 ns.

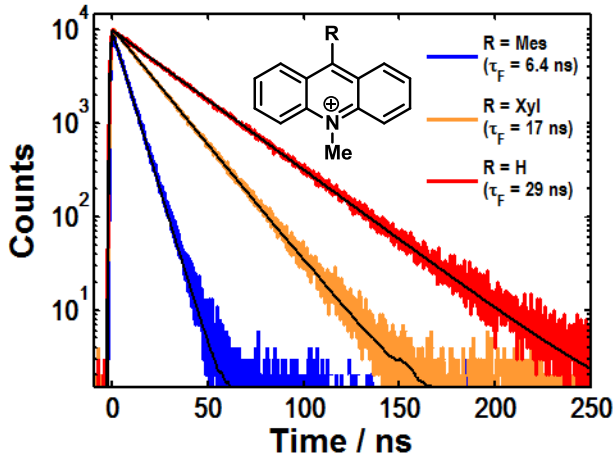

Figure S5. Fluorescence lifetime of several 10-methyl-acridinium tetrafluoroborate salts measured at 515 nm by Time-Correlated Single Photon Counting (TCSPC). The decays are fit to a monoexponential (black traces) after reconvolution with the instrument response profile.

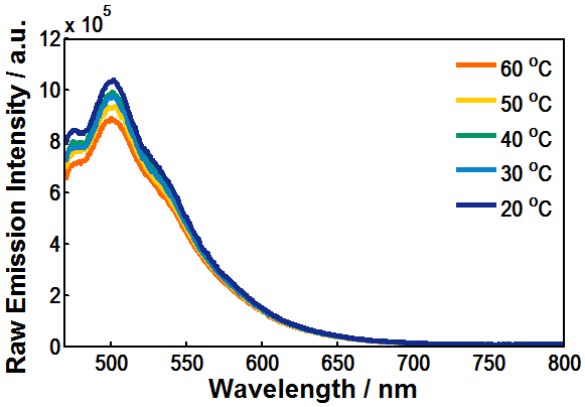

Figure S6. Raw variable temperature fluorescence spectra of **Xyl-Acr$^+$** in DCE.

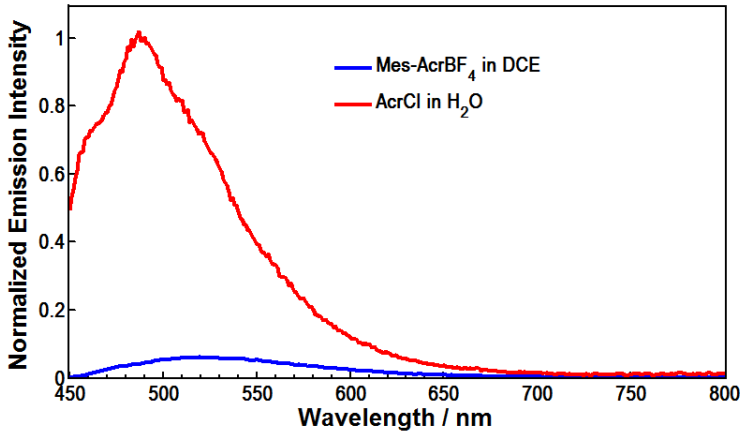

Figure S7. Absorbance corrected fluorescence spectra for **Mes-AcrBF$_4$** and **AcrCl** for the determination of the relative quantum yield of fluorescence (Φ_F) for **Mes-Acr$^+$** in DCE. The absolute quantum yield of fluorescence for **AcrCl** in H_2O is 1.0,[6] and Φ_F for **Mes-Acr$^+$** is calculated by dividing the integrated area beneath the blue curve by the integrated area beneath the red curve. Φ_F is calculated to be 0.08 or 8% for **Mes-Acr$^+$** in DCE.

VI. Stern-Volmer Analyses

Stern-Volmer experiments were conducted with detection at 515 nm, where the solutions in DCE contained Mes-AcrBF$_4$ (1.60×10^{-5} M) and a quencher ranging from 3.0×10^{-4} to 1.7×10^{-2} M in concentration. Comparison of UV-Vis absorption spectra taken before and after lifetime quenching studies verified that **Mes-Acr**$^+$ was unchanged. Stern-Volmer analysis was conducted according to the following relationship:

$$\frac{\tau_o}{\tau} = \mathbf{1} + \boldsymbol{K_{SV}}[\boldsymbol{Q}] = \mathbf{1} + \boldsymbol{k_q}\boldsymbol{\tau_o}[\boldsymbol{Q}] \qquad \text{(eq. S2)}$$

where τ_o and τ are the fluorescence lifetime in the absence and presence of quencher Q, K_{SV} is the Stern-Volmer constant, k_q is the bimolecular quenching constant, and [Q] is the concentration of quencher. An example of the fluorescence lifetime with increasing [Q] is shown in Figure S8 (Q = anethole = **An**).

Calculation of Gibbs Energy for Photoinduced electron transfer:

$$\boldsymbol{\Delta G_{ET} = f[E_{p/2}(Q/Q^{+\bullet}) - E_{p/2}(\text{Mes-Acr+/Mes-Acr}\bullet) - E_{0,0}]} \qquad \text{(eq. S3)}$$

$\boldsymbol{f}$ **= 23.061 kcal mol^{-1} eV^{-1}**
$\boldsymbol{E_{p/2}}$**(Mes-Acr$^+$/Mes-Acr•) = -0.55 V**
$\boldsymbol{E_{0,0}}$**=2.67 eV** (see **Figure S3**)

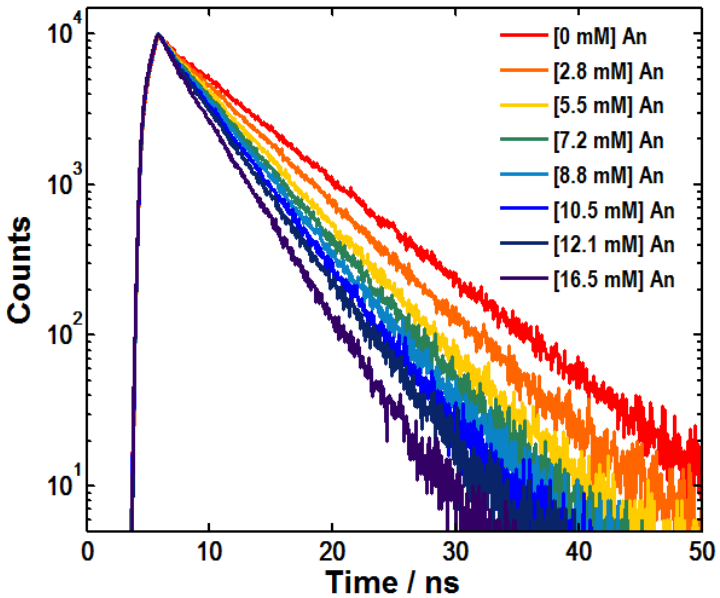

Figure S8. Fluorescence lifetime of **Mes-Acr**$^+$ (16 µM in DCE) measured at 515 nm at the concentrations of anethole (**An**) given.

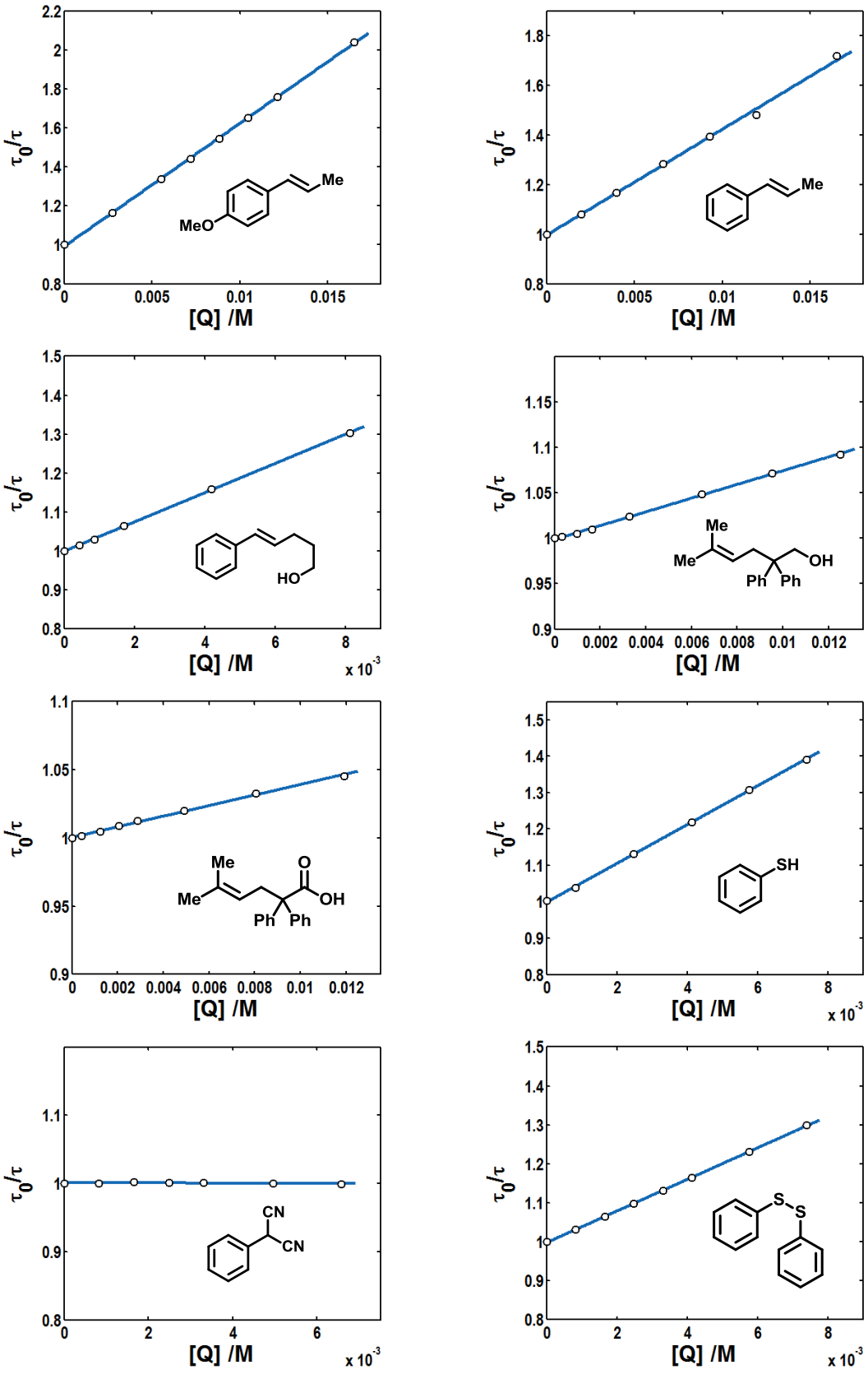

Figure S9. Stern-Volmer plots of quenching of **Mes-Acr**$^{+}$ (16 μM) fluorescence lifetime for each quencher studied. Fluorescence lifetime was measured by TCSPC with detection at 515 nm (20 nm bandwidth). The Stern-Volmer quenching constant, K_{SV}, was determined by the slope of the linear regression (R^2 > 0.99), where the bimolecular quenching constant, k_q, is equal to K_{SV}/τ_o.

VII. Laser Flash Photolysis/Transient Absorption experiments

Laser Flash Photolysis/Transient Absorption was performed using the commercially available LP920 system by Edinburgh Instruments, Inc., and the identical system used has been described elsewhere.[8] Laser excitation was provided by a pulsed Nd:YAG laser in combination with an optical parametric oscillator (OPO) for wavelength selection. Probe light was generated by a 450 W Xe lamp, which was pulsed at a rate of 1 Hz. Typical experiments employed laser excitation at 430 nm (3.5 $\pm$ 0.1 mJ, 5-7 ns fwhm) with single wavelength transient absorption monitored at the indicated wavelengths (0.3-2.0 nm bandwidths) with a photomultiplier tube (PMT) and transient spectra recorded using a gated CCD at the indicated time delays (10 ns gate width) unless otherwise indicated. The probe light was passed through a 380 nm long-pass filter before reaching the sample to minimize higher energy excitation. A 435 nm long pass filter was placed between the sample and detector for single-wavelength measurements to suppress laser scatter. When collecting transient absorption spectra, only a 380 nm long-pass filter was applied to the probe light. For all records, the probe background was collected between laser shots and subtracted from the signal, and fluorescence background was subtracted where relevant. Transient absorption kinetics were fit with the equations described below using the Levenberg-Marquardt algorithm as implemented in Matlab.

A. With Mes-Acr$^+$

Laser flash photolysis was performed on a 50 μM solution of Mes-AcrBF$_4$ in DCE. Transient absorption spectra were collected at time delays ranging from 20 ns to 200 μs. Verhoeven reports first order (mono-exponential) decay[7] of the microsecond transient for Mes-AcrPF$_6$ in MeCN, while Fukuzumi reports second-order behavior of the transient.[9] In our hands, wide variation was seen when applying a mono-exponential kinetic model to fit the decay of the microsecond transient at wavelengths ranging from 460 to 600 nm. Transient absorption studies conducted immediately after sample preparation in a rigorously oxygen-free glovebox yielded a first-order decay constant of τ = 38 μs for the signal at 480 nm (Figure S11a). Yet, analysis of the residuals indicates that the mono-exponential model does not adequately describe the signal decay. Considering that Fukuzumi reports second order behavior due to formation of a triplet-triplet dimer,[10] we attempted to fit the transient absorption at 480 nm with a second order kinetic model; however, a satisfactory fit could not be obtained (Figure S11b). Intriguingly, the best fit is obtained when the signal is fit to a kinetic model with both mono-exponential and second-order terms (Figure S11c), possibly indicating that the triplet **T** decays from both the triplet-triplet dimer and the free triplet simultaneously. Importantly, decay of **T** at longer wavelengths (i.e., wavelengths greater than ~570 nm) consistently follows monoexponential decay with τ_T = 45 µs, even while higher-order decay components are detected at 480 nm. Parallel studies with samples allowed to stand for greater than 1 hour saw in increasingly diminished lifetimes at all wavelengths, due to the difficulty in completely excluding O_2 from screw-cap sealed cuvettes. With the cuvette open to air, measured lifetimes dropped below τ = 5 µs, consistent with the notion that the microsecond transient is a triplet.

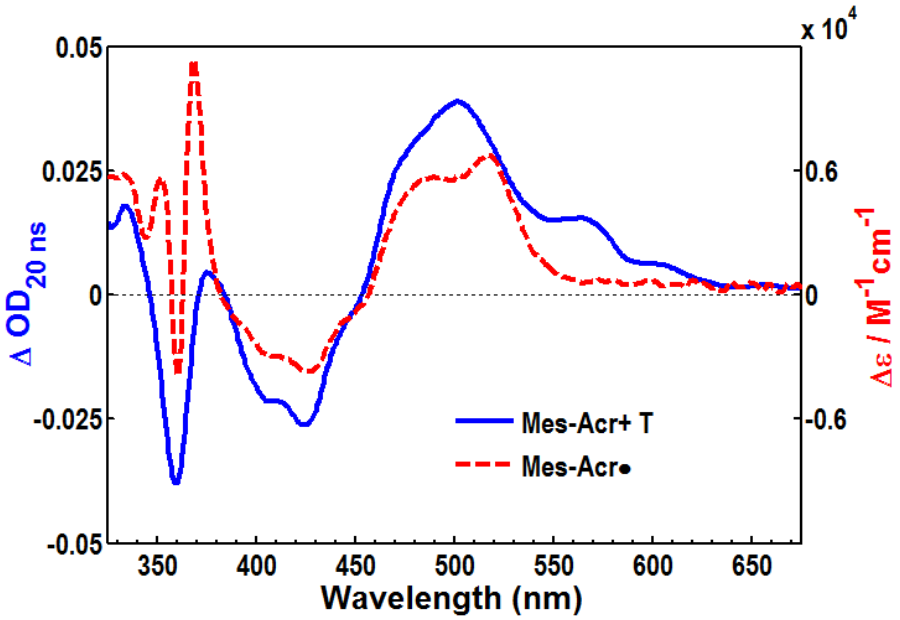

Figure S10. Transient absorption spectrum (blue) for **Mes-Acr$^+$ T** (50 μM in DCE) taken at 20 ns with laser excitation at 430 nm. Difference spectrum for **Mes-Acr•** shown as calculated from spectroelectrochemical records (dashed red).

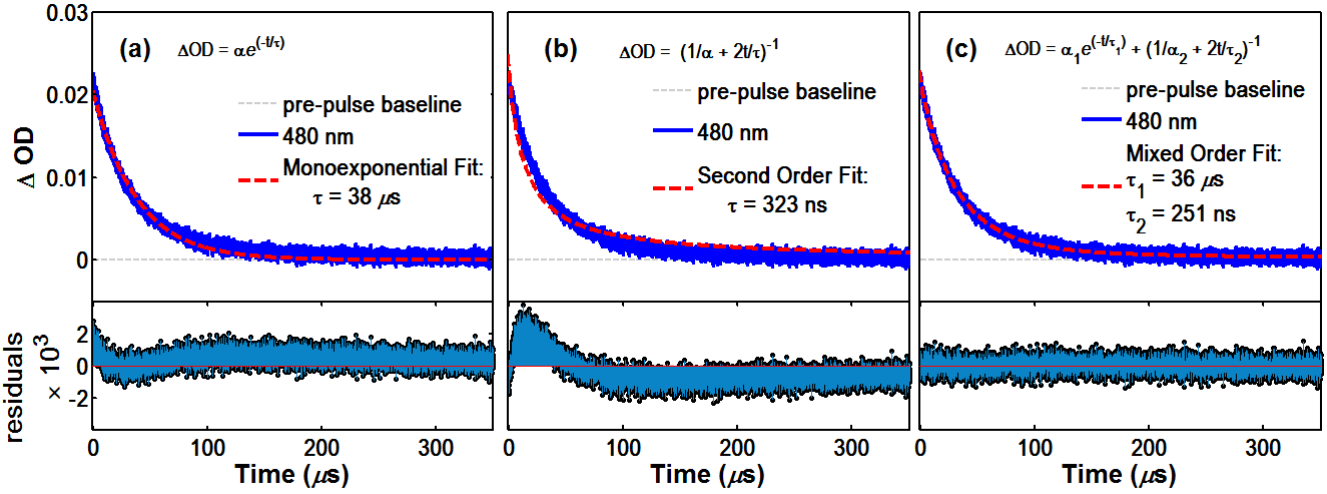

Figure S11. Transient absorption kinetics for **Mes-Acr$^+$** (50 μM in DCE) measured at 480 nm with laser excitation at 430 nm. Fit to **(a)** monoexponential decay: $\Delta\mathbf{OD_{480}}(t) = \boldsymbol{\alpha e}^{-\frac{t}{\tau_T}}$, **(b)** second order decay: $\Delta\mathbf{OD_{480}}(t) = \frac{1}{\frac{1}{\alpha_0} - 2\frac{t}{\tau}}$ (second order fit: α_o fixed at 0.023 in order to obtain a reasonable fit), and **(c)** a mixed order kinetic model with exponential and second-order decay terms: $\Delta\mathbf{OD_{480}}(t) = \boldsymbol{\alpha_1 e}^{-\frac{t}{\tau_1}} + \frac{1}{\frac{1}{\alpha_2} + 2\frac{t}{\tau_2}}$.

B. With Mes-Acr$^+$/Alkene Cation Radicals:

Mes-Acr$^+$ concentration in DCE was 5.0 × 10^{-5} M (in all cases, absorbance at 430 nm was less than 0.5) for detection of styrenyl cation radicals, with a typical alkene concentration of 5 to 10 × 10^{-3} M. Transient absorption spectra are corrected to subtract fluorescence at time delays where significant (i.e., t < 100 ns). Transient emission spectra were recorded for **Mes-Acr**$^+$ using the same system with excitation at 430 nm (see above Figure S4).

Electron transfer from anethole to singlet **Mes-Acr**$^{+*}$ is efficient; thus, the transient absorption spectrum at 500 ns contains little contribution from **T**. The differential absorption spectrum for anethole-cation radical is calculated by normalizing the difference spectrum of **Mes-Acr•** at 520 nm to the observed transient absorption at 500 ns, then subtracting **Mes-Acr•** from the 500 ns spectrum. When LFP is conducted with **Mes-Acr**$^+$ and β-methylstyrene (**βMS**), (*E*)-5-Phenylpent-4-en-1-ol (**R-OH**), and *tert*-Butyldimethyl-(*E*)-(5-phenylpent-4-enyloxy)silane (**R-OTBDMS**), the transient absorption spectrum at 20 ns contains significant contribution from the T in addition to the feature on the low energy side corresponding to the styrenyl cation radical. The spectrum for **T** (Figure S10, blue) was normalized to the observed absorbance at 460 nm (isosbestic point for **Mes-Acr•** difference spectrum), and this normalized **T** spectrum was subtracted. The difference spectrum for **Mes-Acr•** was then normalized to the absorbance at 520 nm (under the assumption that the alkene cation radical does not possess a significant absorbance at 520 nm). Subtraction of the normalized **Mes-Acr•** spectrum yields the absorbance of the **βMS**, **R-OH**, and **R-OTBDMS** cation radicals.

The lifetime of each cation radical was determined by analysis of the single wavelength kinetic decay at 590 nm. In all cases, the signal at 590 nm contains a contribution from **T**, which decays with a time constant τ_T = 45 μs, relatively unchanged from records where alkenes are absent. For **βMS** and alkene **R-OTBDMS** the decay is fit with a biexponential function:

$$\Delta \mathbf{OD}_{590}(t) = \alpha_T e^{-\frac{t}{\tau_T}} + \alpha_{CR} e^{-\frac{t}{\tau_{CR}}} \qquad \text{(eq. S4)}$$

where τ_T corresponds to decay of **T** and τ_{CR} corresponds to decay of the respective cation radical. Alkene **R-OH**, however, is fit with a single exponential function corresponding to **T** decay, confirming that cation radical absorption for **R-OH** is essentially completely quenched before the first time point (40 ns). A lower boundary for the rate of cyclization k_2 can be estimated as 2.5 × 10^7 s^{-1} (i.e., 1/τ = 1/(40 ns) or 1/4.0×10^{-8} s).

Previous studies examining quenching of the triplet **T** have demonstrated quenching of the decay lifetime (at 480-520 nm) of **T** at increasing quencher concentrations. The best kinetic model describing the native decay of **T** in DCE contains 2 terms (Figure S11c), and an additional term would be necessary to describe the contribution from **Mes-Acr•**. Additionally, the native decay of **T** is likely to be perturbed when **Mes-Acr•** is present, as **T** is capable of oxidizing **Mes-Acr•**. Thus, we recognized that we could not obtain reliable rate quenching information, because multiple species absorb at the wavelengths of interest. We do, however, show this signal decay at 520 nm for three concentrations of **βMS** (Figure S15). The decay is approximately mono-exponential with a residual signal at t = 400 μs attributed to the persistent radical **Mes-Acr•**. After subtracting the residual signal at t = 400 μs for each decay, it is clear that the signal

intensity is diminished at increasing quencher concentration. Although the lifetime of the decay is relatively unchanged, that the magnitude of the transient is diminished can be rationalized by fast reductive quenching of either a singlet state or the triplet by **βMS.**

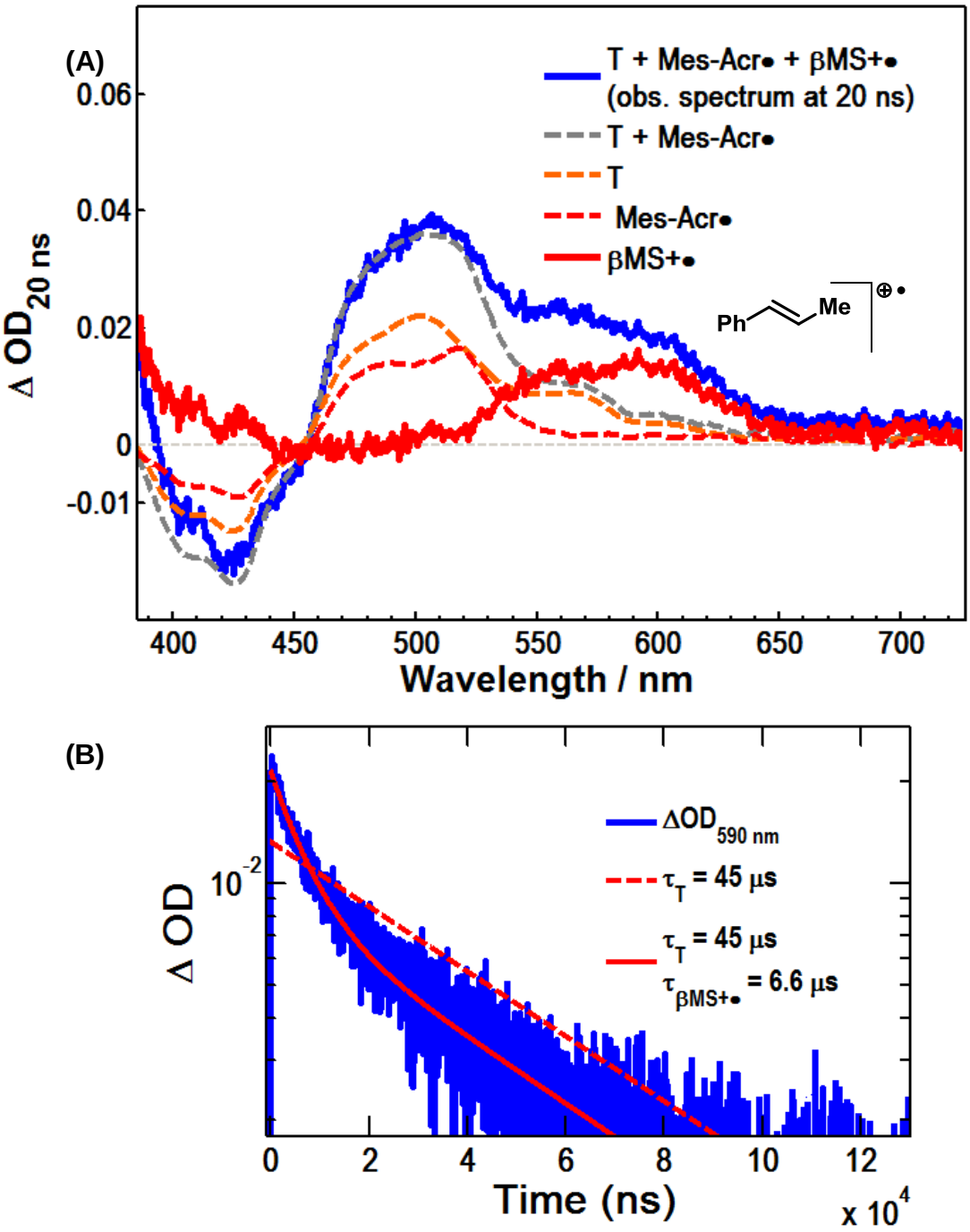

Figure S12. Detection of the β-methylstyrene cation radical by LFP of a DCE solution containing Mes-AcrBF$_4$ (50 μM) and β-methylstyrene (**βMS**, 6 mM). **(a)** Transient absorption spectra showing the contributions of **Mes-Acr$^+$ T** (orange), **Mes-Acr•** (dashed red), and βMS$^+$• (red). Subtraction of the combined contributions of T and **Mes-Acr•** (gray) give the absorption spectrum for βMS$^+$•. **(b)** Transient absorption kinetics at 590 nm showing the observed signal (blue) fit to a biexponential (solid red) where one decay constant is identical to that of **Mes-Acr$^+$ T**, while the other corresponds to the decay of the cation radical **βMS$^+$•** at τ = 6.6 μs.

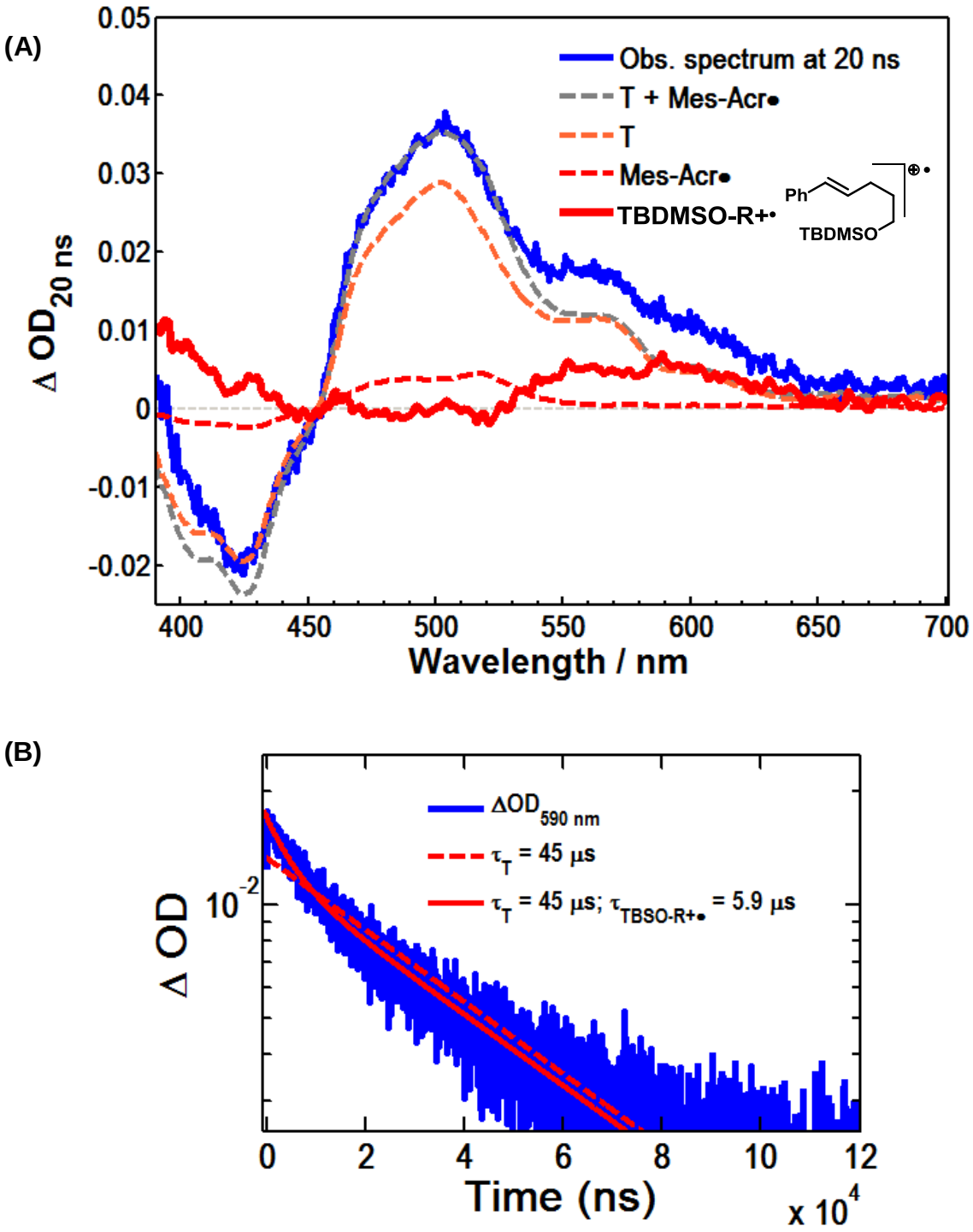

Figure S13. Detection of the cation radical **R-OTBDMS**$^{+}$• by LFP of a DCE solution containing Mes-AcrBF$_4$ (50 μM) and **R-OTBDMS** (6 mM). **(a)** Transient absorption spectra showing the contributions of **Mes-Acr**$^{+}$ **T** (orange), **Mes-Acr•** (dashed red), and **R-OTBDMS**$^{+}$• (red) are shown. Subtraction of the combined contributions of **T** and **Mes-Acr•** (gray) give the absorption spectrum for **R-OTBDMS**$^{+}$• (red, smoothed with Savitsky-Golay filter with a 3rd order polynomial and a frame size of 11). **(b)** Transient absorption kinetics at 590 nm showing the observed signal (blue) fit to a biexponential (solid red) where one decay constant is identical to that of **Mes-Acr**$^{+}$ **T**, while the other corresponds to the decay of the cation radical **R-OTBDMS**$^{+}$• at τ = 5.9 μs.

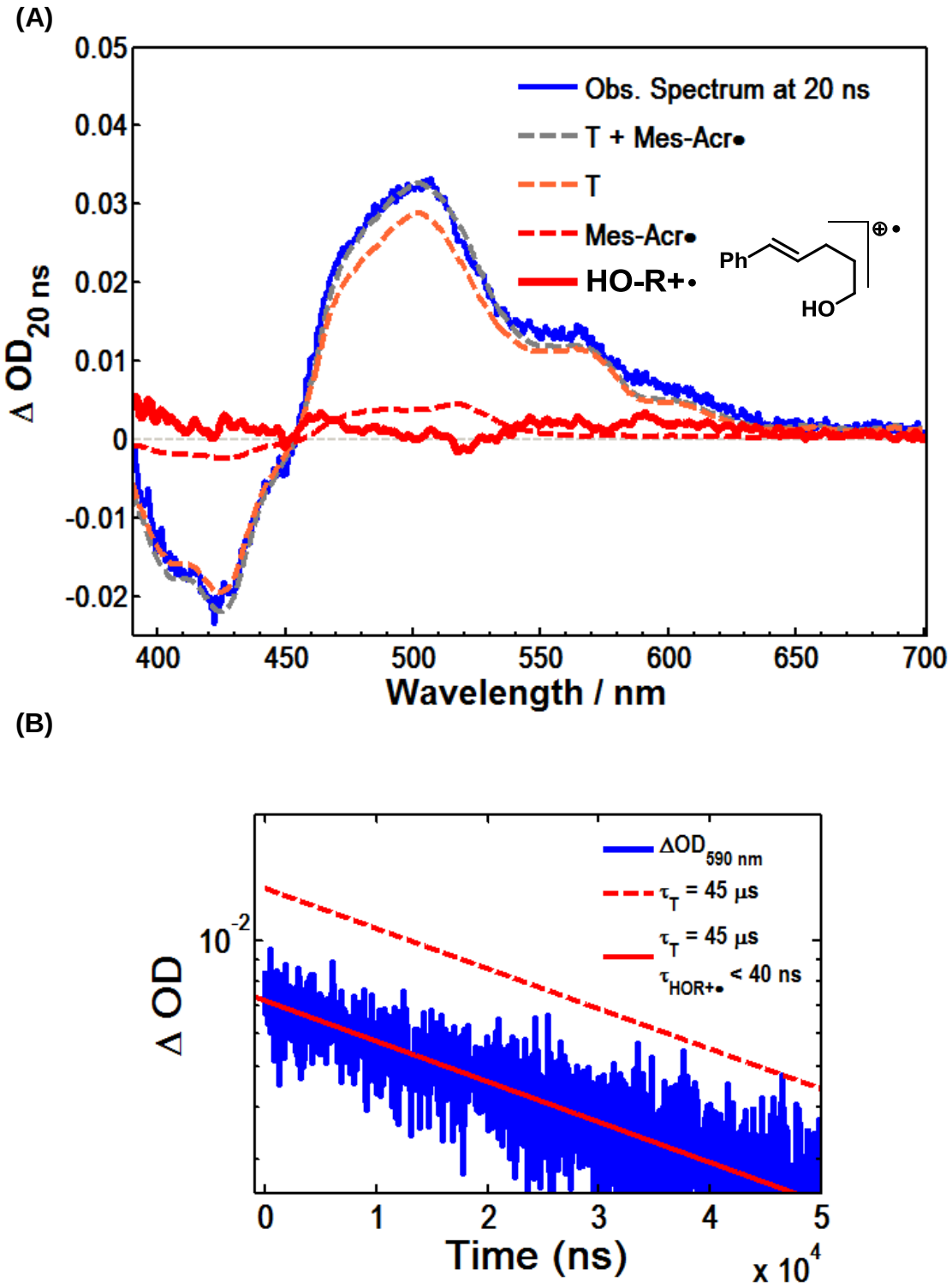

Figure S14. Detection of the cation radical **ROH^{+}•** by laser flash photolysis of a DCE solution containing Mes-AcrBF$_4$ (50 μM) and alkenol **ROH** (6 mM). **(a)** Transient absorption spectra showing the contributions of **Mes-Acr^{+} T** (orange), **Mes-Acr•** (dashed red), and **ROH^{+}•** (red) are shown. Subtraction of the combined contributions of **T** and **Mes-Acr•** (dashed gray) give the absorption spectrum for **ROH^{+}•** (red, smoothed with Savitsky-Golay filter with a 3rd order polynomial and a frame size of 11). **(b)** Transient absorption kinetics at 590 nm showing the observed signal (blue) fit to a monoexponential (solid red). The decay constant is identical to that of **Mes-Acr^{+} T**, confirming that the cation radical **ROH^{+}•** is consumed before the response time of the instrument (40 ns) in this experiment.

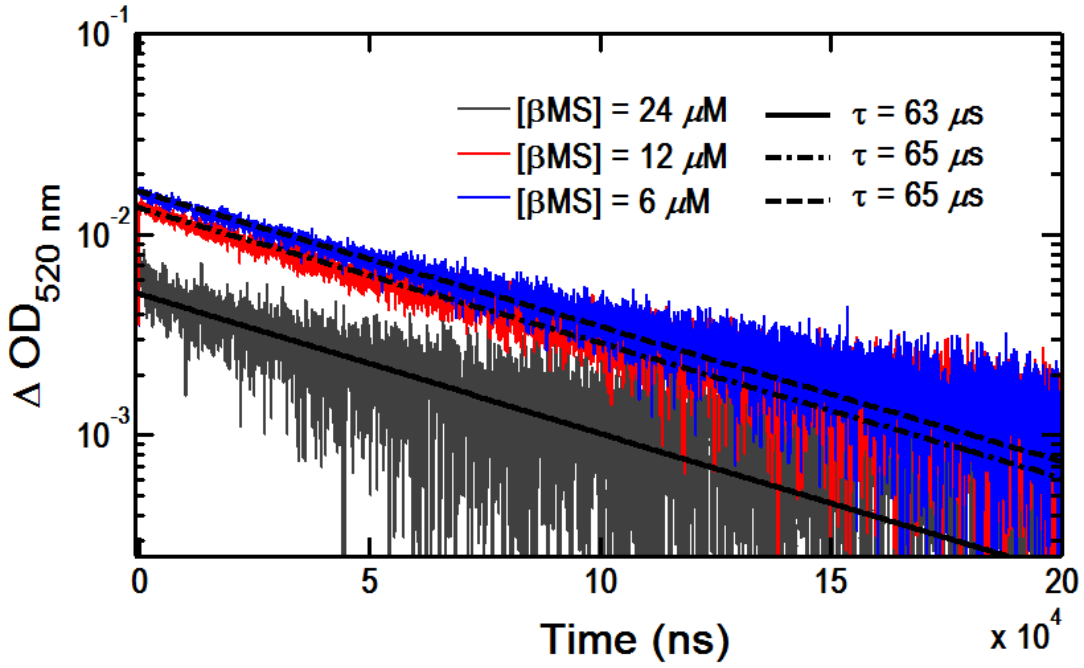

Figure S15. Dependence of transient absorption kinetics for **Mes-Acr**$^+$ (75 μM in DCE) with **βMS** (6 to 24 mM) measured at 520 nm with laser excitation at 430 nm. In all cases, the residual signal at longer time delays after **T** has decayed (t > 350 μs) has been subtracted and is attributed to **Mes-Acr·**. This subtraction of the **Mes-Acr·** contribution is an approximation assuming that the concentration of **Mes-Acr·** is invariant with time, although, based on the redox potentials of **T** and **Mes-Acr·,** electron transfer is feasible, if not likely. the contribution of **Mes-Acr·** to the signal at 520 nm is determined by the residual signal at t = 400 μs. After subtraction of this constant, the transient signals are modeled by monoexponential decay: $\Delta\mathbf{OD}_{\mathbf{520\ nm}}(\boldsymbol{t}) = \boldsymbol{\alpha e^{-\frac{t}{\tau}}}$.

C. Studies involving Mes-Acr•

i. Chemical Reduction of Mes-Acr$^+$ to Mes-Acr• using $CoCp_2$

A 50 μM solution of 9-mesityl-10-methyl-acridinyl radical (**Mes-Acr•**) and bis-cyclopentadiene Cobalt (III) tetrafluoroborate (**CoCp**$_2^+$) in DCE was prepared as follows: in a dry, nitrogen filled glovebox, stock solutions of both Mes-AcrBF$_4$ (10 mM) and **CoCp**$_2$ (20 mM) were prepared by dissolving 20.0 mg Mes-AcrBF$_4$ (5.01×10^{-5} mol) and **CoCp**$_2$ (1.00×10^{-4} mol) separately in 5.00 mL DCE each. In a 4 mL quartz cell (nominal volume, StarnaCells), 20.0 μL of the Mes-AcrBF$_4$ stock solution was diluted to a total volume of 4.00 mL for a concentration of [**Mes-Acr**$^+$] = 50 μM. To this solution was slowly added 10.0 uL **CoCp**$_2$ stock solution while swirling. Upon addition of **CoCp**$_2$, the pale yellow **Mes-Acr**$^+$ solution immediately became light pink in color. Following complete addition of **CoCp**$_2$, the cell was sealed with a Teflon lined screw cap and the solution swirled excessively to ensure complete mixing. The cell was removed from the glovebox and immediately analyzed by UV-Vis absorption spectroscopy. Complete conversion of **Mes-Acr**$^+$ to the corresponding acridinyl radical was confirmed by comparison of the absorption spectrum to that of **Mes-Acr•** generated electrochemically (see above). The extinction coefficient of the chemically generated **Mes-Acr•** (~7000 M^{-1} cm^{-1}) matches the value calculated from spectroelectrochemistry. Contribution from the oxidized cobaltocene (**CoCp**$_2^+$) to this absorption spectrum was assumed to be very small in the wavelength range of interest. This assumption is supported by literature precedent indicating that the molar extinction coefficient of the cobaltocenium species ($\varepsilon_{400\text{-}600nm} < 300$ $M^{-1}cm^{-1}$) is <5% compared to **Mes-Acr•** in the visible.[11,12]

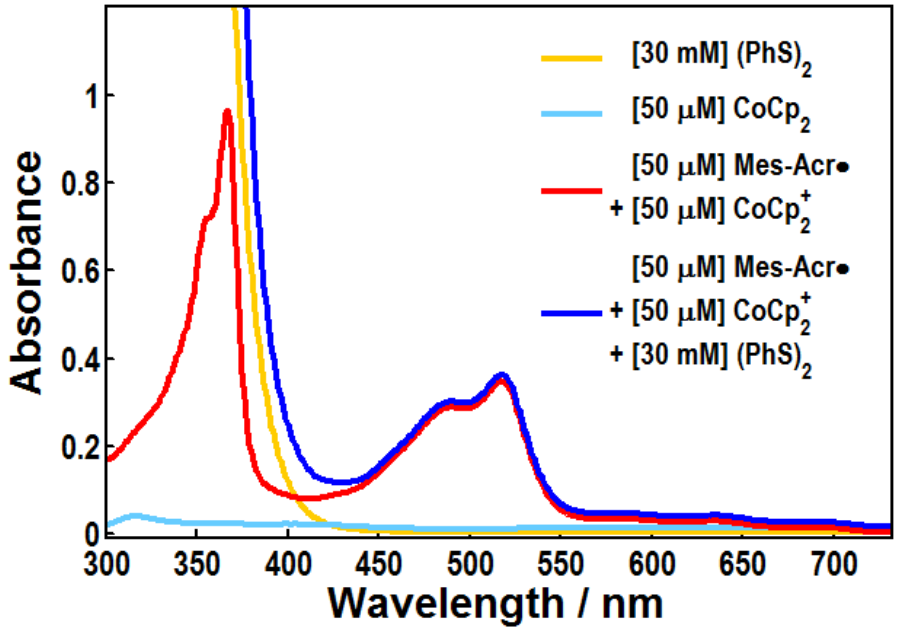

Figure S16. UV-Vis absorbance spectra for species relevant to Laser Flash Photolysis experiments involving **Mes-Acr•** oxidation.

ii. Mes-Acr• consumption by LFP-generated PhS•

Solutions of **Mes-Acr•**/**CoCp**$_2$BF$_4$ containing phenyl disulfide (**PhS**)$_2$ were prepared as described above, with the additional step of adding a microliter quantity of (**PhS**)$_2$ stock solution to the cell prior to mixing with **CoCp**$_2$ ([(**PhS**)$_2$] = 30 mM). This solution was kept in the dark until analysis by UV-vis. The resulting UV-vis absorption spectrum closely resembles that of **Mes-Acr•**/**CoCp**$_2$BF$_4$ (50 μM) with the additional feature of the broad absorption extending into the far UV due to (**PhS**)$_2$. Comparison to the individual spectra of (**PhS**)$_2$ and **Mes-Acr•**/**CoCp**$_2$BF$_4$ precludes the existence of any additional species resulting from a possible background reaction between (**PhS**)$_2$ and **Mes-Acr•** or **CoCp**$_2$BF$_4$. Laser flash photolysis with excitation at 410 nm was performed on this solution in the quartz cell with an average laser pulse energy of 7.0 mJ. A 380 nm long pass optical filter was placed between the probe source and the sample, and a 435 nm long pass filter was placed between the sample and detector. Kinetic absorption at wavelengths 445 nm and 520 nm were collected with 3-5 laser shots, after which point the net photochemical outcome became non-negligible. New solutions were used for each kinetic measurement, as well as for measurement of the transient difference spectrum taken at 30 μs. Control experiments where (**PhS**)$_2$ is excluded reveal no transient signal differing from baseline absorbance. Laser Flash photolysis with a solution of (**PhS**)$_2$ (3.0×10^{-2} M) confirmed that **PhS•** could be generated with laser pulses at this wavelength.

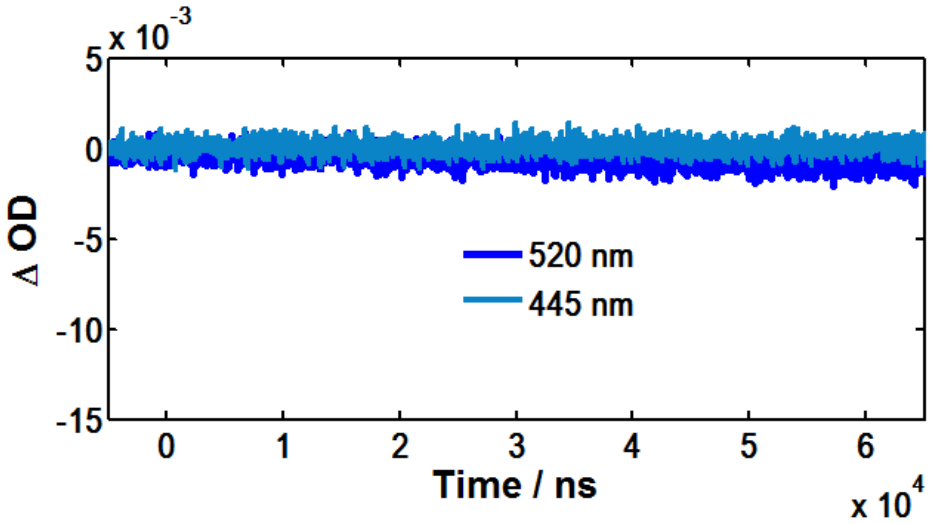

Figure S17. Laser flash photolysis (λ_{ex} = 410 nm, 8.0 mJ) of **Mes-Acr•**/**CoCp**$_2$BF$_4$ (50 μM) containing no (**PhS**)$_2$. The absence of an appreciable ΔOD at either wavelength supports the conclusion that bleaching at 520 nm and appearance of a signal at 445 nm is due to electron transfer to **PhS•**.

Kinetic fitting for the 520 nm transient was fit to a single exponential function of the form

$$\Delta \mathbf{OD}_{520}(t) = \alpha_1(1 - e^{-k_{obs}t}) \quad \text{(eq. S5)}$$

$$\textbf{where } k_{obs} = 2.5\times10^5 \text{ s}^{-1}$$
$$\alpha_1 = -0.0096$$

This corresponds to a final resting concentration [**Mes-Acr•**]$_\infty$ (i.e., at time delays greater than 50 μs) of:

$$[\textbf{Mes-Acr•}]_\infty = \alpha_1/_{\Delta\varepsilon_{(\textbf{Mes-Acr•, 520 nm})}\times\ell} \quad \text{(eq. S6)}$$
$$= -0.0095/-6610 \text{ M}^{-1}\text{cm}^{-1}\times 1.00 \text{ cm}$$
$$= 1.4\times10^{-6} \text{ M}$$

The signal at 445 nm is fit to an equation of the form

$$\Delta \mathbf{OD}_{445}(t) = \alpha_2\left(1 - e^{-k_{obs}t}\right) + \alpha_3 e^{-k_{obs}t} + \frac{1}{\frac{1}{\alpha_4}+2k_r t} \quad \text{(eq. S7)}$$

$$k_{obs} = 2.5\times10^5 \text{ s}^{-1}$$
$$2k_r = 3.5\times10^6 \text{ M}^{-1}\text{s}^{-1}$$
$$\alpha_2 = 0.0022$$
$$\alpha_3 = 0.0020$$
$$\alpha_4 = 0.0003$$

Discussion of eq. S7: The pseudo-first order rate constant k_{obs} describes both the appearance of **Mes-Acr$^+$** and the decay of **PhS•** in the bimolecular electron transfer reaction. This rate constant is identical to that obtained by fitting the signal bleach at 520 nm. The second order rate constant $2k_r$ describes decay of **PhS•** by a competing bimolecular recombination pathway, which is confirmed to follow second order kinetics in separate experiments (Figure S18a).

The pre-exponential factor α_2 corresponds to the concentration of **Mes-Acr$^+$** reached after **PhS•** is completely consumed ($_\Delta\varepsilon_{(\textbf{Mes-Acr}^+,\ 445\ nm)}\times\ell$ = 2200 M^{-1}, [**Mes-Acr$^+$**]$_\infty$ = ~1.0 ×10^{-6} M). The sum of the pre-exponential factors α_3 and α_4 ($\alpha_3 + \alpha_4$ = 0.0023) corresponds to the concentration of **PhS•** formed upon irradiation with the laser pulse ($_\Delta\varepsilon_{(\textbf{PhS•},\ 445\ nm)}\times\ell$ = 2000 M^{-1},[13] [**PhS•**]$_o$ = ~1.2×10^{-6} M). Although this scenario requires a more sophisticated model to truly describe the mixed order kinetics of **PhS•** decay, we make the simplification that the pseudo-first order and second order decay modes are separate, where the initial concentration of **PhS•** in each decay term is specified by α_3 and α_4, respectively, and the molar extinction coefficient of **PhS•**. Under this assumption, approximately 85% of the initially formed **PhS•** is consumed in the pseudo-first order reaction ([**PhS•**]$_o$(1st) = ~1.0×10^{-6} M) and 15% is consumed through bimolecular recombination ([**PhS•**]$_o$(2nd) = ~0.2×10^{-6} M).

It should be noted that [**Mes-Acr•**]$_\infty$ and [**Mes-Acr$^+$**]$_\infty$ as calculated from α_1 and α_2, respectively, are expected to be identical, however, some discrepancy is noted. Monitoring at 520 and 445 nm were performed with different samples, and due to the fact that each measurement is the average of only 3-5 laser shots, even small variation in laser pulse energy is expected to give rise to differences in the quantity of **PhS•** generated between experiments. Variation in [**PhS•**]$_o$ is expected to only affect the final concentration [**Mes-Acr$^+$**]$_\infty$ and not the observed rate of **Mes-Acr$^+$** appearance since [**Mes-Acr•**]$_o$ (50 μM) is in large excess of [**PhS•**]$_o$ (0.9-1.3 μM) under these conditions.

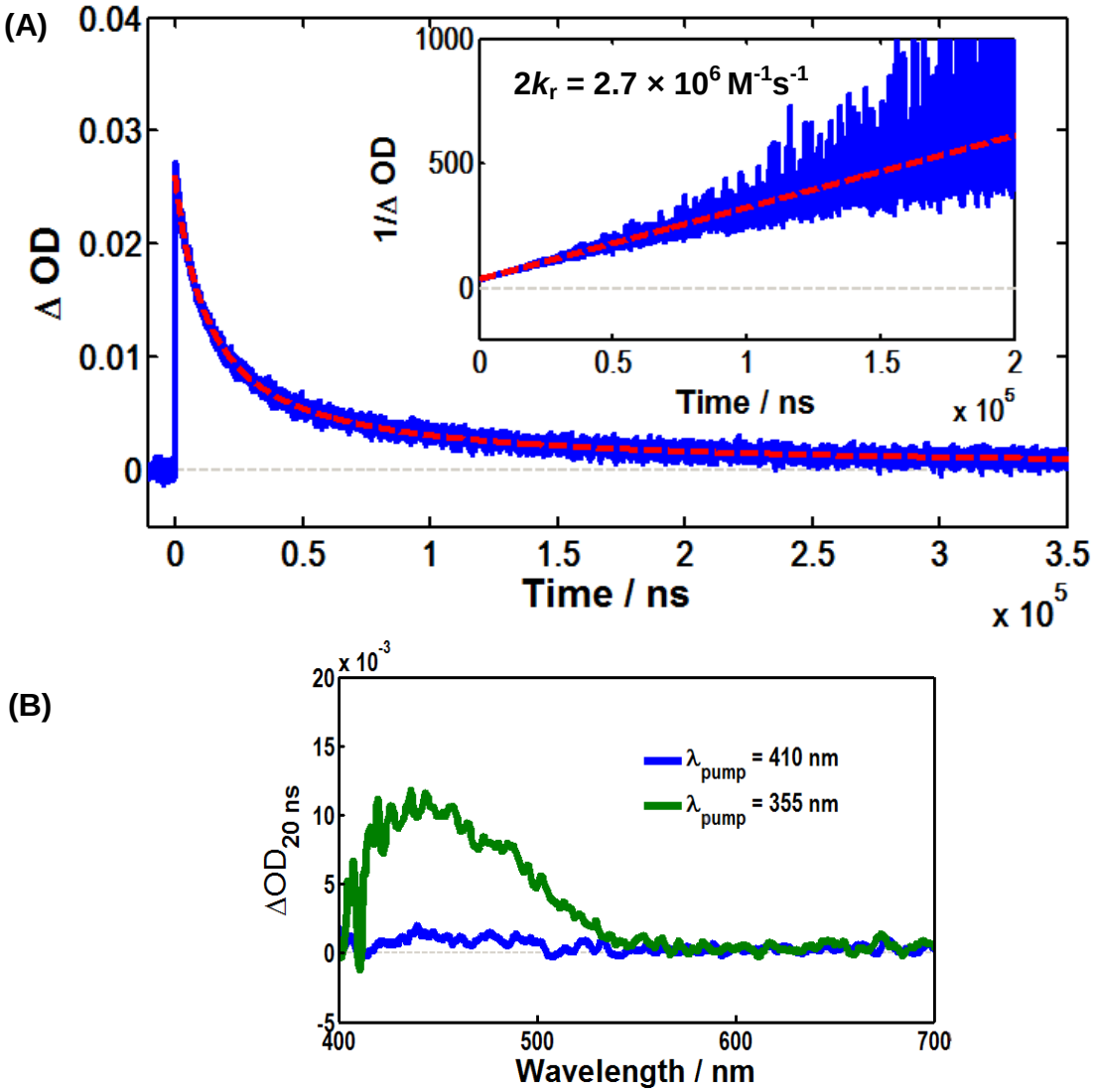

Figure S18. Laser flash photolysis with in DCE: **(a)** Transient decay of signal at 460 nm by second order kinetics, corresponding to recombination of **PhS•**; [(**PhS**)$_2$] = 30 mM, λ_{pump}= 355 nm **(b)** Transient absorption spectra measured at a 20 ns time delay; green: [(**PhS**)$_2$] = 3 mM; blue: [(**PhS**)$_2$] = 30 mM.

Solutions used in the pseudo-first order study on the rate of **Mes-Acr•** oxidation were prepared in a glovebox as described above, wherein the total volume of the solution was 10 mL. **Mes-Acr**· concentrations in DCE ranged from 2.5 × 10^{-5} to 2.5 × 10^{-4} M, and the concentration of (**PhS**)$_2$ was 3.0 × 10^{-3} M. This disulfide concentration was found to give optimal photolytic yield of **PhS•** = ca. 5 µM at a laser excitation wavelength of 355 nm. Solutions were prepared in flame-dried 20 mL vials sealed with a rubber septum and PTFE tape. Upon removal from the glovebox, the rubber septa were not punctured until introduced into a quartz flow cell through a stainless steel needle connected to the flow cell by FEP tubing. The flow rate through the cell

was controlled by positive pressure from a dry, rigorously oxygen free Argon stream, such that each laser pulse irradiated a fresh solution. The average laser pulse energy was 8.0 mJ at 355 nm. For all trials, a 380 nm long pass filter was placed between the probe source and the sample and also between the sample and detector. The reported transient signals with detection at 520 nm are the average of 3-5 laser shots and are fit to a single exponential function as described above (eq. S5).

Based on the molar extinction coefficient reported for **PhS•** at 460 nm (~2000 $M^{-1}cm^{-1}$), the observed transient absorption at 460 nm (ΔOD = 0.010) for LFP on a solution of $(\mathbf{PhS})_2$ in DCE was used in estimating the maximum concentration of **PhS•** to be roughly 5 μM upon disulfide photolysis. This is in good agreement with the observation that the ΔOD reaches a minimum of -0.040 over the range of **Mes-Acr•** concentration (see Figure S19 below), corresponding to the consumption of approximately 5-6 μM **Mes-Acr•**. Thus, under these conditions, **Mes-Acr•** is in large excess of **PhS•**.

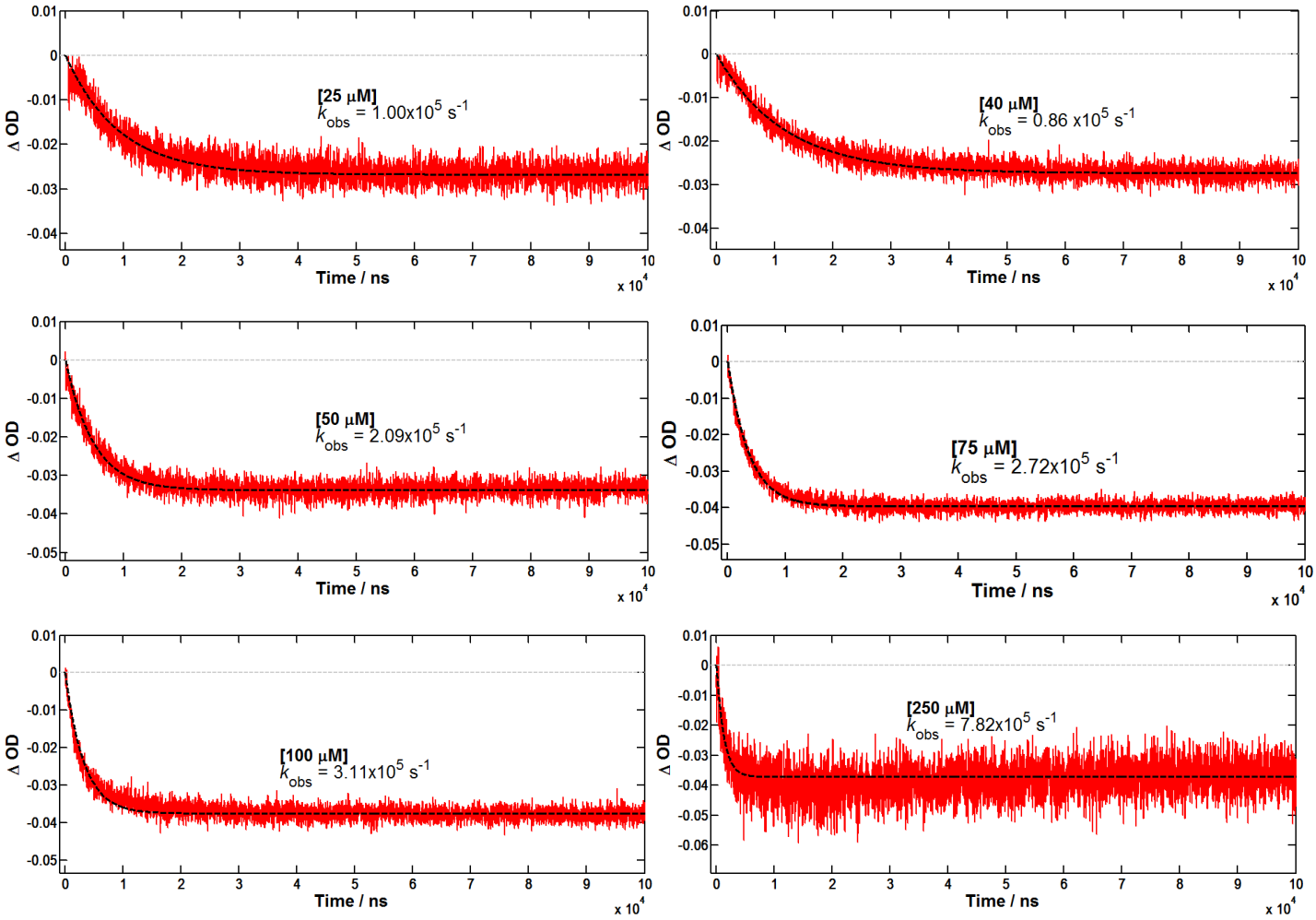

Figure S19. Transient absorption signals at 520 nm showing consumption of **Mes-Acr•** at increasing rate when [**Mes-Acr•**] is increased. The rate of decay k_{obs} is found by fitting the decay curves to eq. S5 (dashed black trace).

VIII. Disulfide Exchange Experiments

Stock solutions of phenyl disulfide and 4-methylphenyl disulfide were prepared by dissolving 27.3 mg (0.13 mmol) and 30.8 mg (0.13 mmol) of each disulfide (respectively) in 5.0 mL DCE, such that the concentration of each stock solution was 2.5×10^{-2} M. To study the kinetics of exchange, 0.5 mL of each disulfide stock solution were mixed in a flame-dried 1 dram vial containing a Teflon-coated magnetic stir bar and sealed with a Teflon coated septum cap. The total concentration of disulfide was 2.5×10^{-2} M. For experiments where Mes-AcrBF$_4$ was included, solutions were prepared by mixing 0.5 mL of each disulfide stock solution with 5.0 mg Mes-AcrBF$_4$ (0.013 mmol), such that the concentration of Mes-AcrBF$_4$ was 1.3×10^{-2} M. After sealing each vial with PTFE tape, the vials were removed from the glovebox and the Teflon septum cap was punctured with a needle supplying positive pressure of dry N_2 for the duration of the experiment to exclude oxygen from the reactions. The solutions were stirred on a magnetic stir plate and irradiated using the setup described above. Aliquots (volume < 5 μL) were removed at the time points listed below without ceasing irradiation, quenched by addition to excess diethyl ether and immediately analyzed on an Agilent 5973 GC-MS system. Prior to experimental analysis, calibration curves for (**PhS**)$_2$ and (**4-Me-PhS**)$_2$ were constructed, and it was determined that the detector response was linear for both disulfides in the range of concentrations relevant in this experiment. Calibration experiments also showed that the detector response factor for (**4-Me-PhS**)$_2$ was 1.3 times that of (**PhS**)$_2$. In the absence of a calibration standard for **4-Me-PhSSPh**, it was assumed that the detector response factor is likewise 1.3 for **4-Me-PhSSPh**. Thus, the integrated areas of (**4-Me-PhS**)$_2$ and **4-Me-PhSSPh** are scaled by a factor of 1/1.3. The theoretical mole fraction of **4-Me-PhSSPh** when 1:1 (**PhS**)$_2$:(**4-Me-PhS**)$_2$ fully exchange to 1:1:2 (**PhS**)$_2$:(**4-Me-PhS**)$_2$:**4-Me-PhSSPh** is

$$\text{mol fraction at equilibrium} = \frac{[\textbf{4-Me-PhSSPh}]}{[(\textbf{PhS})_2] + [(\textbf{4-Me-PhS})_2] + [\textbf{4-Me-PhSSPh}]} = 0.5 \qquad \text{(eq. S8)}$$

Thus, the ratio of mixed to total unmixed disulfide is 1:1. Therefore, conversion to an equilibrium amount of 50 mol% **4-Me-PhSSPh** was determined by the expression

$$\text{conversion} = \frac{[\textbf{4-Me-PhSSPh}]}{[(\textbf{PhS})_2] + [(\textbf{4-Me-PhS})_2]} = \frac{[\text{area } \textbf{4-Me-PhSSPh}] / 1.3}{[\text{area } (\textbf{PhS})_2] + [\text{area } (\textbf{4-Me-PhS})_2] / 1.3} \qquad \text{(eq. S9)}$$

where the area was found by baseline-to-baseline integration of each peak using ChemStation software. Control experiments were performed where **(a)** light was excluded by wrapping the vial in aluminum foil and placed side-by-side with the irradiated vials or **(b)** light was excluded and the vial heated to 50 ^{o}C in an oil bath. Both control experiments **(a)** and **(b)** contained 0.013 M (**PhS**)$_2$ + 0.013 M (**4-Me-PhS**)$_2$ and the total volume of the solution was 1.0 mL (as above). In both cases, a negligible amount of (**4-Me-PhS**)$_2$ (mol fraction <0.004) was formed by 400 minutes; therefore, we consider these background reactions to be of negligible consequence.

Table S1. Disulfide exchange amounts as determined by GC-MS

No Mes-AcrBF$_4$		w/ 0.013 M Mes-AcrBF$_4$	
time / min	$\frac{[p\text{-Me-PhSSPh}]}{[(p\text{-Me-PhS})_2] + [(PhS)_2]}$	time / min	$\frac{[p\text{-Me-PhSSPh}]}{[(p\text{-Me-PhS})_2] + [(PhS)_2]}$
0	0.00	0	0.00
5	0.04	5	0.14
10	0.11	10	0.30
25	0.30	25	0.55
45	0.56	45	0.69
75	0.95	75	0.85
115	1.00	115	1.03
240	1.06	240	0.99

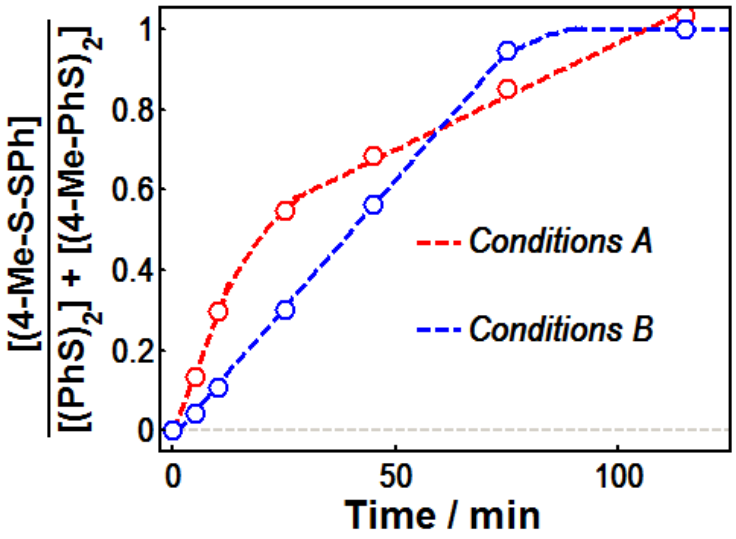

Figure S20. Plot showing formation of mixed disulfide (**4-Me-PhSSPh**) under the photolytic conditions: (A) [Mes-AcrBF$_4$] = 0.013 M (B) no Mes-AcrBF$_4$. The rate to equilibrium concentration of (**4-Me-PhSSPh**) is zero-order when Mes-Acr$^+$ is excluded, indicating a direct homolytic mechanism for generation of PhS· from (PhS)$_2$.

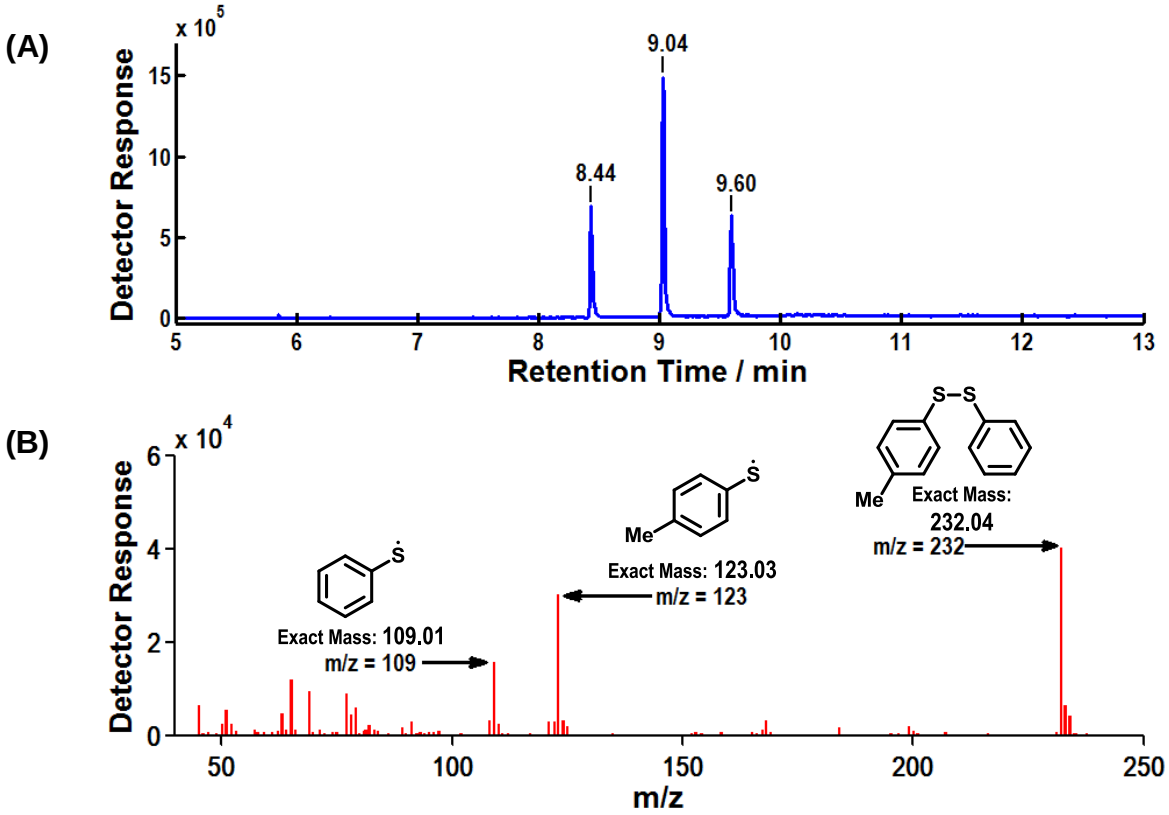

Figure S21. (a) Example Gas Chromatogram of an aliquot after *t* = 240 min showing (**PhS**)$_2$ (retention time = 8.44 min), (**4-Me-PhSSPh**) (retention time = 9.04 min), and (**4-Me-PhS**)$_2$ (retention time = 9.60 min). **(b)** Example mass spectrum corresponding to **4-Me-PhSSPh** (peak with retention time = 9.04 min) showing m/z = 232 for the parent mixed disulfide, and fragments at m/z = 109 and 123 for the fragments **PhS** and **4-Me-PhS**, respectively.

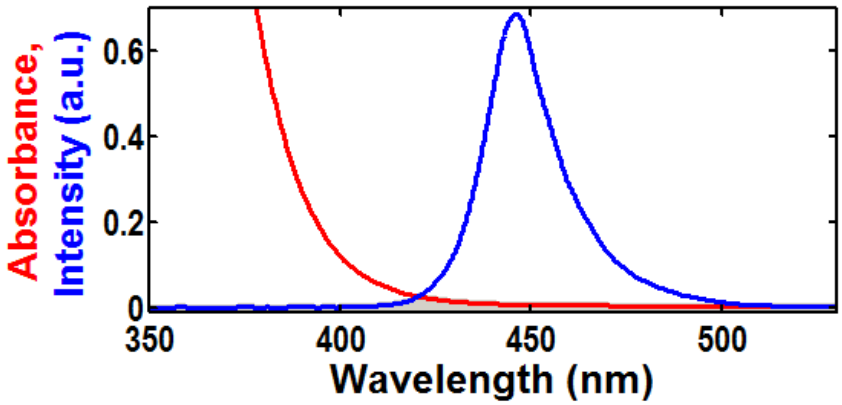

Figure S22. Absorbance spectrum of 30 mM (**PhS**)$_2$ in DCE (red) overlaid with the spectral output for the Ecoxotic LED lamp used in photolysis (blue, arbitrary units). The overlap between the traces is highlighted in gray. An Ocean Optics HR4000 spectrometer (Dunedin, FL) was used to measure the emission spectrum of the LED lamp, which was directly oriented toward the aperture of the spectrometer unit at a distance of approximately 10 cm.

IX. Reaction Progress Monitoring

A. Gas Chromatography: Alkenol ROH/Product/PhSH/$(PhS)_2$

Time-monitored conversion was measured by analyzing aliquots with gas chromatography (Agilent 6850 Series II, flame ionization detector).

In a glovebox, two solutions of total volume 1.1 mL DCE were prepared in flame-dried 1 dram borosilicate glass vials with a PTFE coated magnetic stir bar and sealed with a PTFE-lined septum cap:

(A) 44.5 mg alkenol **ROH** [0.25 M], 5.6 µL **PhSH** [0.05 M], 5.5 mg Mes-AcrBF_4 [0.013 M], 61 µL dodecane [0.25 M] (internal standard)

(B) 44.5 mg alkenol **ROH** [0.25 M], 5.9 mg (**PhS**)$_2$ [0.025 M], 5.5 mg Mes-AcrBF_4 [0.013 M], 61 µL dodecane [0.25 M] (internal standard)

After sealing each vial with PTFE tape, the vials were removed from the glovebox and the Teflon septum cap was punctured with a needle supplying positive N_2 pressure to exclude oxygen from the reactions. The solutions were stirred on a magnetic stir plate and irradiated using a single LED lamp. Aliquots (volume < 5 µL) were removed at the time points listed below without ceasing irradiation, and immediately quenched by dilution with 0.5 mL diethyl ether. Each sample was analyzed by GC within 18 hours, although the makeup of each sample was not found to change upon standing under ambient conditions for a greater period (i.e., 24 hours). Peak areas were found using the OpenLab Software, and were scaled according to the detector response factor for each analyte. The detector response was determined for alkenol **ROH**, the corresponding tetrahydrofurane product, **PhSH**, and (**PhS**)$_2$ as a burn ratio relative to dodecane (**DD**) as an internal standard. The burn ratio of dodecane to both **ROH** and product was found to be linear when [**DD**]:[**ROH**] and [**DD**]:[**pdt**] ranged from 1 to 0. The conversion was normalized by setting [**DD**]:[**ROH**] at time = 0 to 100%.

B. UV-Vis Spectroscopy: Mes-Acr$^+$/Mes-Acr· monitoring during photolysis

Time-evolution spectra were recorded on a Varian Cary 50 spectrophotometer with a scan rate of 1200 nm/min (time resolution is estimated to be ca. 0.5 min).

In a glovebox, two solutions of total volume 2.0 mL DCE were prepared in quartz cells with a PTFE-coated magnetic stir bar and sealed with a PTFE-lined septum cap:

(A) 81.0 mg alkenol **ROH** [0.25 M], 10.2 μL **PhSH** [0.05 M], 10.0 mg Mes-AcrBF$_4$ [0.013 M]

(B) 81.0 mg alkenol **ROH** [0.25 M], 10.7 mg (**PhS**)$_2$ [0.025 M], 5.5 mg Mes-AcrBF$_4$ [0.013 M]

After sealing each cell with a Teflon coated screwcap, the vials were removed from the glovebox and analyzed by UV-Vis while irradiating with a blue LED lamp and continuous stirring. Spectra were collected from 300 to 800 nm with a 1 nm step size and a scan rate of 1200 nm per minute. A spectrum was collected prior to irradiation (t = 0) and at subsequent intervals following the start of irradiation (all intervals greater than 1 minute). The cell was irradiated with an incidence perpendicular to the light path of the instrument in order to minimize scatter. It should be noted that although the same lamp was employed in this photolysis as in the experiments described above, the intensity of the light reaching the solution is not likely to be identical to the preparative photolysis conditions, due to the differing materials and shapes of each vessel. However, since **A** and **B** were run under identical conditions (i.e., solution volume, stir rate, distance from lamp to cell are all unchanged), comparison between **A** and **B** is valid. Additional UV-Vis experiments were conducted in the same way as described above, with the exception that the photolysis lamp was turned off upon observation of complete consumption of both **Mes-Acr$^+$** and **Mes-Acr·** (ca. 5 min). Spectra were recorded for an additional 8 hours after the lamp was removed and the cell shielded from ambient light.

X. Determination of Association Constant for Donor-Acceptor Complex

UV-VIS absorption spectra were collected for solutions of 455 μM **Mes-AcrBF$_4$** containing **βMS** in the concentrations listed in Figure S23. The Donor-Acceptor complex is detected as a weak new feature on the low energy side of the **Mes-Acr$^+$** absorption. The ΔAbsorbance spectra (spectrum where [**βMS**] = 0 M subtracted from the spectrum for each sample) reveal that the new absorption is centered around 467 nm. The equilibrium constant K_{DA} is defined as K_{DA} = [**DA**]/[**βMS**][**Mes-Acr$^+$**] where **DA** is assumed to be a binary complex between **βMS** and **Mes-Acr$^+$**. K_{DA} is calculated by the Benesi-Hildebrand method[14,15] according to the equation

$$\frac{[\text{Mes}-\text{Acr}]_o}{\Delta\text{Abs}_{467\text{nm}}} = \frac{1}{\varepsilon_{DA}K_{DA}} \cdot \frac{1}{[\beta\text{MS}]} + \frac{1}{\varepsilon_{DA}} \qquad \text{(eq. S10)}$$

where ε_{DA} is the molar extinction coefficient of **DA**. The best fit line to a plot of [**Mes-Acr$^+$**]/ΔAbs_{467nm} vs. [**βMS**]$^{-1}$ (Figure S24) gives ε_{DA} as the reciprocal of the y-intercept, and K_{DA} is obtained as 0.96 M^{-1}.

It should be noted that the Benesi-Hildebrand method is typically calculated using Absorbance, not ΔAbsorbance as we have done here. However, this method assumes that only the **DA** complex absorbs at the wavelength in question. As **DA** clearly overlaps with the absorption for **Mes-Acr$^+$** in this case, using Abs_{467} rather than ΔAbs_{467} is unsuitable.[15] In order to validate the above calculation, we also calculated K_{DA} by the method of Nash[16] using Absorbance values, which accounts for **Mes-Acr$^+$** absorbance. By the Nash method, we calculate K_{DA} = 1.1, which is within reason of the value calculated by the Benesi-Hildebrand method.

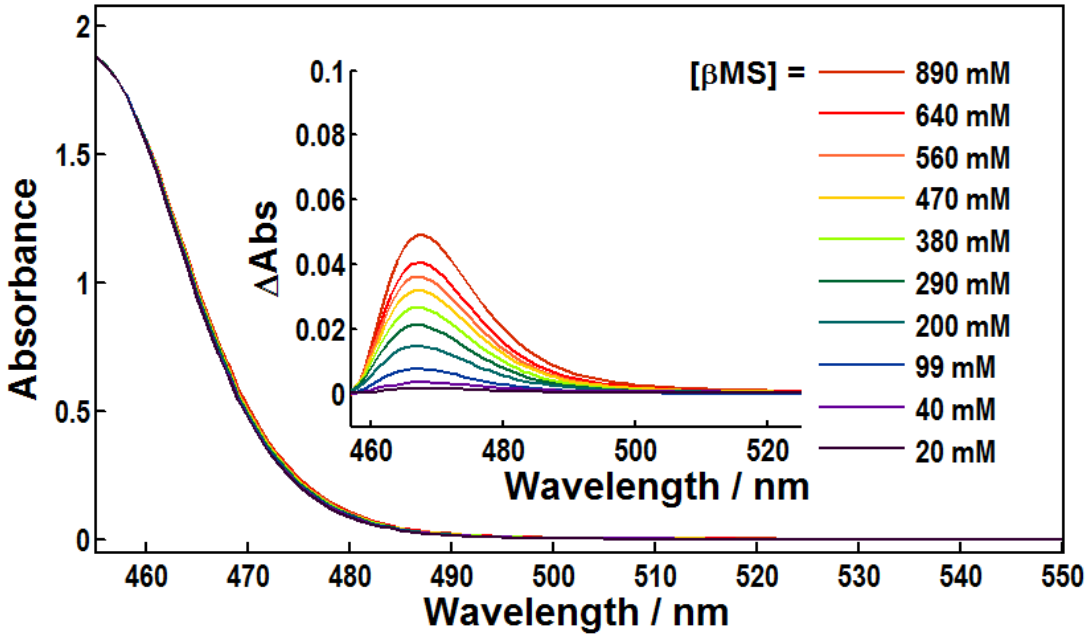

Figure S23. Absorption spectra for solutions of **Mes-AcrBF$_4$** in DCE (455 μM) with **βMS**. Inset shows ΔAbsorbance to emphasize the shape of the new absorption.

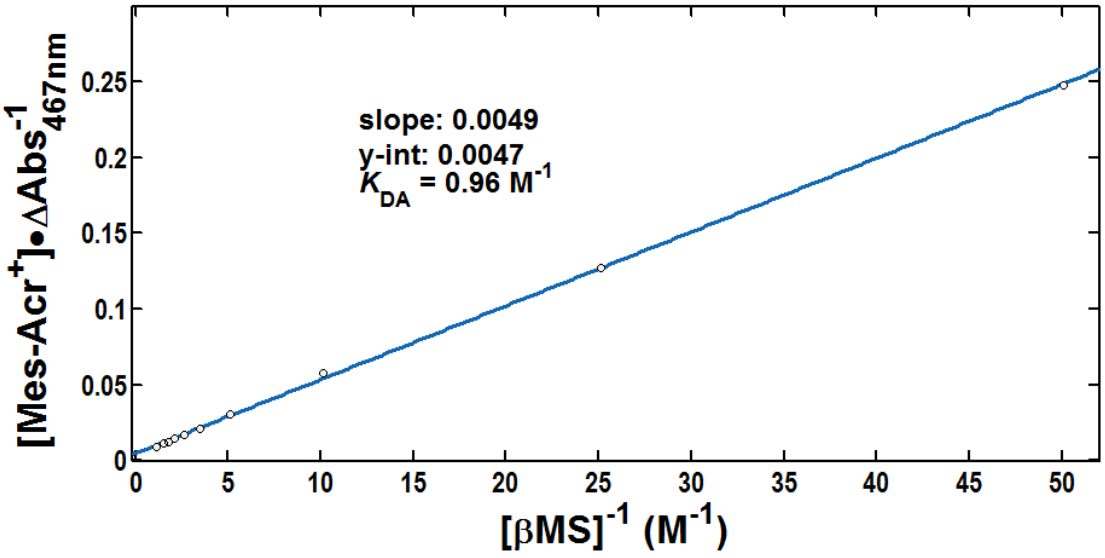

Figure S24. Benesi-Hildebrand plot for the calculation of K_{DA} by equation S10.

XI. Determination of Quantum Yield of Reaction Using Ferrioxalate Actinometry

Potassium ferrioxalate (**$K_3Fe(C_2O_4)_3$**) was prepared as the trihydrate by the known method[17] and recrystallized three times from H_2O. A 0.15 M aqueous solution (1.0 mL) of **$K_3Fe(C_2O_4)_3$** was irradiated for 60 seconds using the identical photolysis setup described above. The number of mol Fe^{2+} was determined from the absorbance at 510 nm of the tris-phenanthroline-Fe^{2+} after developing the photolyzed solution with a buffered solution of 1,10-phenanthroline.[18] Based on the molar extinction coefficient at 510 (ε_{510} = 11,110 $M^{-1}cm^{-1}$)[19] and the absolute quantum yield for photolysis of **$K_3Fe(C_2O_4)_3$** at 457.9 nm (Φ = 0.85),[19] the photon flux was determined to be 6.43×10^{-7} mol photon s^{-1}. Quantum yield of reaction Φ_R was calculated at a given time point using the kinetic data presented in Figure 8 of the text as Φ_R = mol pdt/mol photon.

XII. Computational Details

All calculations were implemented in the Gaussian 09 software package,[20] and were performed at the UB3LYP level of theory[21,22] using the 6-311+G(d) basis set[23,24] with solvation in DCE evaluated in a self-consistent reaction field (SCRF) with the PCM model.[25] Geometry optimization for structures **SM-a**, **SM-b**, **PDT-a** and **PDT-b** yielded the geometries shown. Transition structures **TS-a** and **TS-b** were located by performing relaxed potential energy scans where the distance between atoms C-12 and H-26 was advanced in 0.1 Å increments. The highest energy structure located from this scan was then submitted to a transition state optimization using the Berny algorithm. Vibrational analysis was performed for all stationary points, where each minimum was confirmed as having only positive vibrational frequencies, and each transition structure possessed a single imaginary frequency. Intrinsic Reaction Coordinate (IRC) calculations in both directions verified that TS structures **TS-a** and **TS-b** led to the minimized structures for the respective reactants and products. Thermochemical values (enthalpies and free energies) at 298.15 K were calculated using scaled vibrational frequencies. Images were generated using the CYLview program.[26] Other possible geometries for HAT transfer were also explored, including the pathways where the HAT catalyst is rotated ~180° about the X-H (X = S in PhSH or C in PMN) bond in the transition state. This pathway was found to be at least 1.5 kcal mol^{-1} higher in energy than the pathway explored herein.

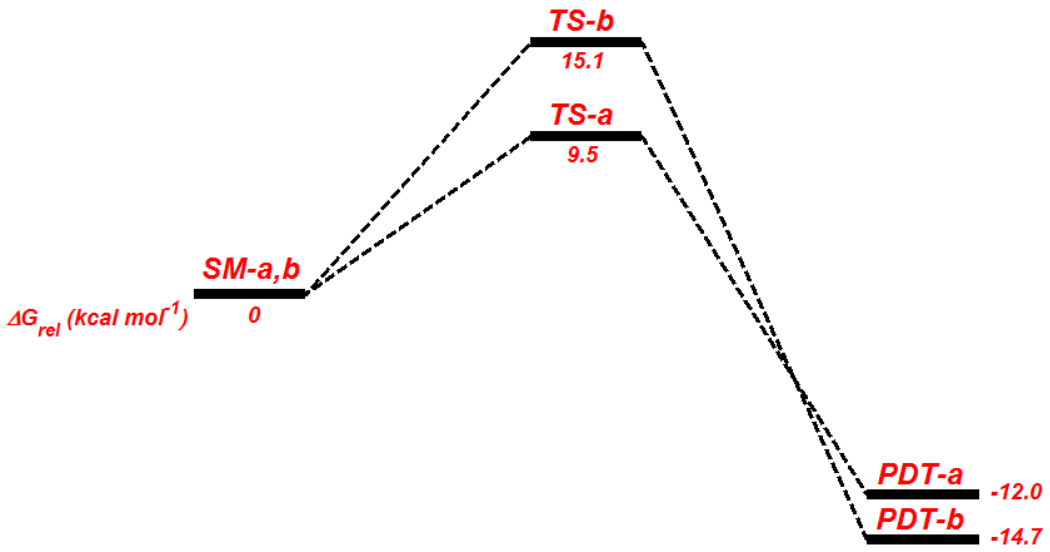

Figure S25. Relative free energies of calculated structures for H-atom transfer.

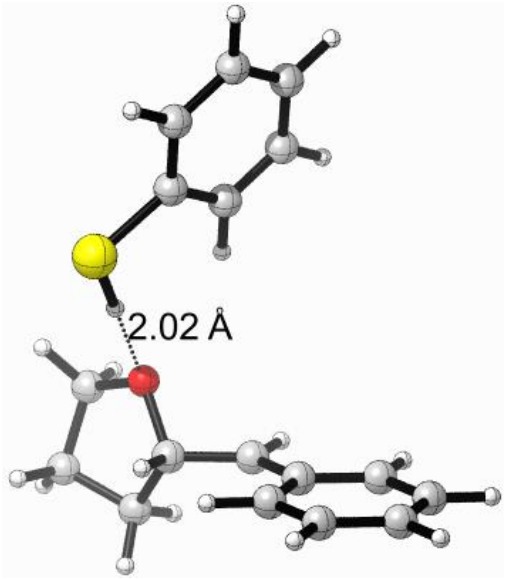

SM-a

H (298 K) = -1132.481289 Hartree ΔH_{rel} **= 0 kcal mol^{-1}**
G (298 K) = -1132.556371 Hartree ΔG_{rel} **= 0 kcal mol^{-1}**

C	-2.9149231	-3.2754902	-0.5724997
C	-2.4914091	-2.0375362	-1.0236827
C	-2.1976641	-0.9730782	-0.1184807
C	-2.3602391	-1.2472462	1.2720133
C	-2.7850671	-2.4913412	1.7111293
C	-3.0673771	-3.5163292	0.7996813
H	-3.1292791	-4.0636752	-1.2874217
H	-2.3774501	-1.8611822	-2.0890787
H	-2.1465611	-0.4776212	2.0044273
H	-2.8970371	-2.6711612	2.7758013
H	-3.3987651	-4.4870332	1.1524413
C	-1.7749581	0.2733418	-0.6328847
H	-1.6736701	0.3640128	-1.7119957
C	-1.4520681	1.5054828	0.1351143
H	-1.4726121	1.3240848	1.2135053
C	-2.3380401	2.7222898	-0.1943247
H	-2.6393961	2.6932218	-1.2461577
H	-3.2424181	2.7382408	0.4163153
C	-1.3971831	3.9042558	0.0645543
H	-1.7000871	4.8163708	-0.4537137
H	-1.3410981	4.1244248	1.1346743
C	-0.0631681	3.3618448	-0.4442537
H	0.0562709	3.5292848	-1.5203247
H	0.8063279	3.7772758	0.0701203
O	-0.0929141	1.9376008	-0.1979567
H	1.3599319	1.2772238	1.0480533
C	3.4740979	-1.1009862	-1.5442687
C	2.7718049	-0.2924832	-0.6513977
C	3.2187389	-0.1583462	0.6689223
C	4.3703329	-0.8408732	1.0801283
C	5.0645849	-1.6464042	0.1794963
C	4.6215639	-1.7816482	-1.1367437
H	3.1176379	-1.1975802	-2.5650437
H	1.8809159	0.2321678	-0.9787377
H	4.7244609	-0.7446032	2.1017223
H	5.9554369	-2.1701862	0.5113543
H	5.1635189	-2.4100212	-1.8354637
S	2.3677599	0.8637008	1.8649743

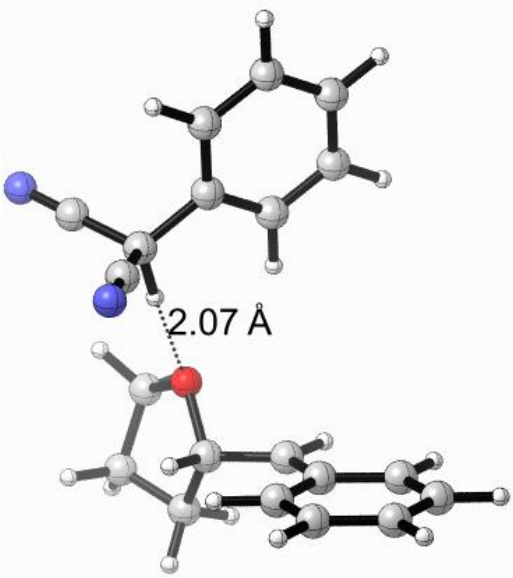

SM-b

H (298 K) = -958.083907 Hartree ΔH_{rel} **= 0 kcal mol^{-1}**
G (298 K) = -958.166656 Hartree ΔG_{rel} **= 0 kcal mol^{-1}**

C	-3.5931702	-2.8629193	-0.6098434
C	-2.9724092	-1.7263963	-1.0981604
C	-2.5352242	-0.6821283	-0.2279704
C	-2.7690162	-0.8666333	1.1671336
C	-3.3912222	-2.0097413	1.6436426
C	-3.8100842	-3.0174403	0.7661246
H	-3.9128732	-3.6387153	-1.2984914
H	-2.8103092	-1.6161303	-2.1662184
H	-2.4551702	-0.1076783	1.8741986
H	-3.5525162	-2.1230703	2.7110606
H	-4.2958512	-3.9089553	1.1477996
C	-1.9118302	0.4605227	-0.7785804
H	-1.7794102	0.4909517	-1.8577864
C	-1.4186142	1.6594547	-0.0488134
H	-1.4755702	1.5220797	1.0344386
C	-2.1179262	2.9783617	-0.4331684
H	-2.4279652	2.9475857	-1.4822744
H	-3.0061782	3.1525817	0.1763706
C	-1.0134012	4.0208507	-0.2284654
H	-1.1833852	4.9427117	-0.7885084
H	-0.9172502	4.2787597	0.8302886
C	0.2218908	3.2656967	-0.7118024
H	0.3447088	3.3493627	-1.7975094
H	1.1494558	3.5845477	-0.2317864
O	-0.0057552	1.8783137	-0.3733354
H	1.4542598	0.8954577	0.7177706
C	2.7511778	-1.8038883	-1.8763154
C	2.2573568	-0.8434923	-0.9926204
C	2.8406978	-0.6958543	0.2659126
C	3.9146638	-1.5059453	0.6422296
C	4.4039048	-2.4628643	-0.2433174
C	3.8229318	-2.6128703	-1.5037554
H	2.2962128	-1.9172043	-2.8544964
H	1.4235488	-0.2113423	-1.2785174
H	4.3718258	-1.3946023	1.6205956
H	5.2380928	-3.0905563	0.0509216
H	4.2060018	-3.3588013	-2.1920314
C	2.2825868	0.3695447	1.2218016
C	1.7298468	-0.2225283	2.4502896
N	1.2778638	-0.6992633	3.3969696
C	3.2891818	1.3883527	1.5605596
N	4.0789248	2.1938857	1.7956596

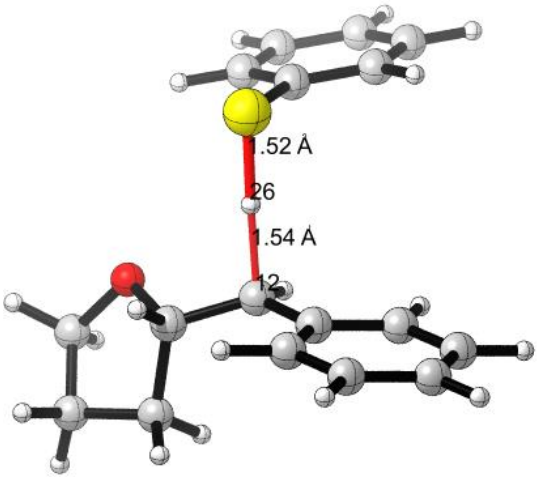

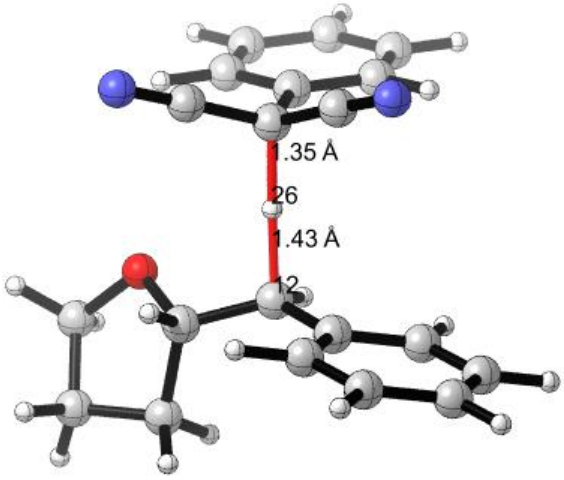

TS-a

H (298 K) = -1132.470444 Hartree **$\Delta H^{\ddagger}$ = 6.8 kcal mol^{-1}**
G (298 K) = -1132.541164 Hartree **$\Delta G^{\ddagger}$ = 9.5 kcal mol^{-1}**

C	-1.9390331	-3.3646772	-0.8389764
C	-1.2110081	-2.1786232	-0.8566844
C	-1.5420501	-1.1005492	0.0029046
C	-2.6306001	-1.2776112	0.8936086
C	-3.3564281	-2.4665942	0.9075146
C	-3.0180611	-3.5161842	0.0429336
H	-1.6691701	-4.1733452	-1.5132594
H	-0.3755611	-2.0665252	-1.5437904
H	-2.9055441	-0.4822912	1.5799296
H	-4.1893431	-2.5785392	1.5968686
H	-3.5870801	-4.4417732	0.0578406
C	-0.7410571	0.1095838	-0.0327204
H	-0.0417211	0.1839048	-0.8683124
C	-1.2791181	1.4430718	0.4158606
H	-1.6827761	1.3753798	1.4373546
C	-2.3586971	2.0394348	-0.5148334
H	-2.1286891	1.7970498	-1.5597824
H	-3.3569511	1.6569418	-0.2844254
C	-2.1974781	3.5434318	-0.2554694
H	-2.5858711	4.1640418	-1.0690974
H	-2.7144551	3.8284368	0.6684996
C	-0.6796461	3.6798108	-0.0898334
H	-0.1837211	3.8732648	-1.0502734
H	-0.3890551	4.4641368	0.6172036
O	-0.2101151	2.4105858	0.4171196
H	0.3522219	-0.1794162	1.0215706
C	4.6172599	0.6161898	-0.2750914
C	3.5194419	0.6518928	0.5889086
C	2.8199809	-0.5281692	0.8955766
C	3.2434839	-1.7432002	0.3296336
C	4.3444079	-1.7748802	-0.5310504
C	5.0331359	-0.5960922	-0.8369104
H	5.1491979	1.5356278	-0.5063864
H	3.1995329	1.5923438	1.0276736
H	2.7090119	-2.6585862	0.5670556
H	4.6630559	-2.7207822	-0.9618664
H	5.8894829	-0.6223142	-1.5056954
S	1.4330179	-0.4949772	2.0264026

TS-b

H (298 K) = - 958.065230 Hartree **$\Delta H^{\ddagger}$ = 11.7 kcal mol^{-1}**
G (298 K) = - 958.140052 Hartree **$\Delta G^{\ddagger}$ = 16.7 kcal mol^{-1}**

C	-3.2100582	-2.4916672	-1.1737931
C	-2.1071872	-1.6483182	-1.1924101
C	-1.9513592	-0.6278762	-0.2270431
C	-2.9463822	-0.5027982	0.7684189
C	-4.0477002	-1.3493692	0.7835909
C	-4.1865862	-2.3472522	-0.1848311
H	-3.3117262	-3.2632802	-1.9297211
H	-1.3531522	-1.7641262	-1.9648321
H	-2.8551642	0.2559418	1.5373999
H	-4.8010642	-1.2354712	1.5560399
H	-5.0473422	-3.0071972	-0.1675541
C	-0.7696762	0.2247378	-0.2736521
H	-0.1855302	0.1356978	-1.1911831
C	-0.7972252	1.6362468	0.2535689
H	-1.1946022	1.6634648	1.2768049
C	-1.5844552	2.6314258	-0.6190101
H	-1.4415852	2.3943608	-1.6778641
H	-2.6540832	2.6127818	-0.4052341
C	-0.9072212	3.9591418	-0.2581181
H	-1.0253772	4.7216728	-1.0303461
H	-1.3216052	4.3561818	0.6727809
C	0.5572948	3.5469798	-0.0668321
H	1.1392928	3.6677258	-0.9859461
H	1.0557448	4.0991058	0.7337459
O	0.5484988	2.1428868	0.2738079
H	0.1876728	-0.4112412	0.5749389
C	4.4083138	-0.1545012	-0.3830991
C	3.3002488	-0.0889642	0.4568919
C	2.3508048	-1.1187322	0.4530389
C	2.5251988	-2.2078172	-0.4113431
C	3.6347388	-2.2667492	-1.2508771
C	4.5808268	-1.2419942	-1.2398071
H	5.1390998	0.6470168	-0.3659161
H	3.1738018	0.7647028	1.1124839
H	1.8020878	-3.0161062	-0.4256191
H	3.7602458	-3.1186072	-1.9106691
H	5.4464708	-1.2915252	-1.8916021
C	1.1256038	-1.0287372	1.3261349
C	0.4847658	-2.2853922	1.6428759
N	-0.0537032	-3.2823192	1.8693269
C	1.2351398	-0.1932302	2.5004799
N	1.2969358	0.4831998	3.4349749

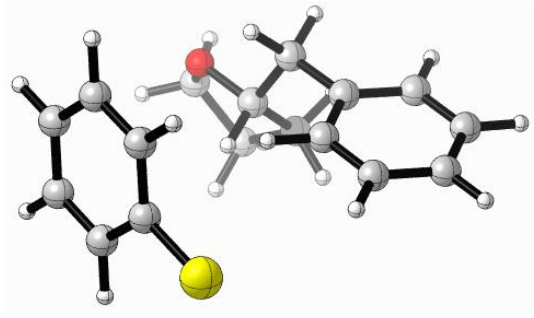

PDT-a

H (298 K) = -1132.496244 Hartree **ΔH_{rxn}= -9.4 kcal mol^{-1}**
G (298 K) = -1132.575477 Hartree **ΔG_{rxn}= -12.0 kcal mol^{-1}**

C	3.2161786	-2.6054878	0.2366049
C	2.9788236	-1.3114398	0.7020759
C	1.6908536	-0.7631578	0.6845039
C	0.6422556	-1.5518798	0.1918919
C	0.8740796	-2.8443848	-0.2766841
C	2.1642736	-3.3761028	-0.2574961
H	4.2226856	-3.0113608	0.2629929
H	3.8056396	-0.7220618	1.0879199
H	-0.3685874	-1.1536508	0.1814949
H	0.0459756	-3.4379378	-0.6514101
H	2.3460696	-4.3832358	-0.6186681
C	1.4344476	0.6499902	1.1608999
H	2.2513416	0.9900122	1.8048379
C	1.2713136	1.6513532	0.0120939
H	0.4558786	1.3133682	-0.6431971
C	2.5192516	1.9311242	-0.8286741
H	3.4111206	1.9243762	-0.1925771
H	2.6638586	1.1953372	-1.6214481
C	2.2425786	3.3448402	-1.3545931
H	3.1473846	3.8826322	-1.6451381
H	1.5820056	3.3053452	-2.2258971
C	1.5303676	3.9996032	-0.1663811
H	2.2373146	4.5064322	0.4999579
H	0.7645016	4.7196462	-0.4667391
O	0.8979646	2.9313032	0.5690589
H	0.5204486	0.6797362	1.7628829
C	-4.1810644	0.2335702	-0.5769201
C	-3.9956424	-0.9769308	-1.2250041
C	-3.8622224	-2.1798828	-0.4819881
C	-3.9254374	-2.1108618	0.9350529
C	-4.1117124	-0.8950408	1.5729319
C	-4.2394134	0.2798732	0.8216099
H	-4.2813634	1.1466192	-1.1536111
H	-3.9499084	-1.0217628	-2.3069441
H	-3.8256164	-3.0249248	1.5087269
H	-4.1580234	-0.8533558	2.6556999
H	-4.3839944	1.2297422	1.3247899
S	-3.6336264	-3.6914468	-1.2826571

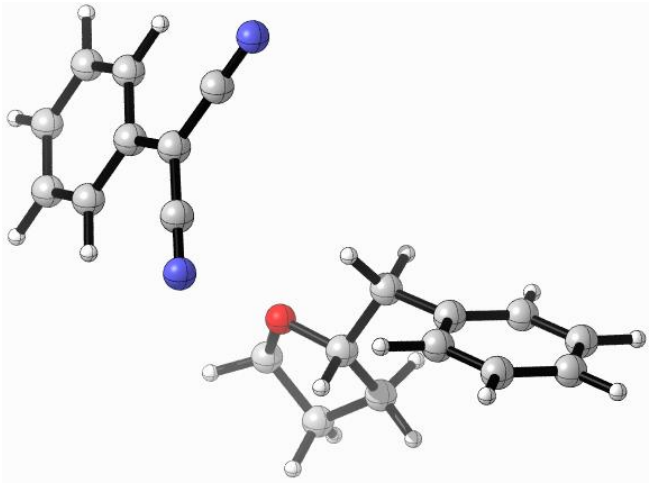

PDT-b

H (298 K) = -958.104217 Hartree **ΔH_{rxn}= -12.7 kcal mol^{-1}**
G (298 K) = -958.190019 Hartree **ΔG_{rxn}= -14.7 kcal mol^{-1}**

C	-4.8216358	-1.9452753	-1.0159654
C	-3.7632788	-1.0700363	-1.2637354
C	-2.6417698	-1.0387783	-0.4265934
C	-2.6075768	-1.9142063	0.6674766
C	-3.6632358	-2.7887733	0.9211866
C	-4.7761898	-2.8071393	0.0793266
H	-5.6793698	-1.9554513	-1.6813044
H	-3.8081538	-0.4068373	-2.1228694
H	-1.7415548	-1.9183243	1.3236396
H	-3.6137838	-3.4604733	1.7725166
H	-5.5969338	-3.4903853	0.2725726
C	-1.5009088	-0.0776973	-0.6801774
H	-1.5265808	0.2795087	-1.7142694
C	-1.5137888	1.1367417	0.2542246
H	-1.4938718	0.7868937	1.2963176
C	-2.6671668	2.1258347	0.0705606
H	-2.9207018	2.2163947	-0.9913744
H	-3.5672968	1.8247537	0.6089746
C	-2.0556478	3.4320447	0.5922236
H	-2.5489928	4.3256897	0.2045566
H	-2.1075658	3.4672867	1.6844606
C	-0.6006498	3.3187277	0.1248496
H	-0.4545698	3.7764067	-0.8599814
H	0.1112312	3.7687477	0.8220216
O	-0.3152398	1.9087677	0.0173476
H	-0.5447038	-0.5933223	-0.5446744
C	4.6117042	1.3379907	0.7680756
C	3.9560222	0.1545617	1.0572646
C	3.9530182	-0.9096643	0.1197066
C	4.6313512	-0.7344663	-1.1136544
C	5.2823382	0.4546717	-1.3895694
C	5.2776682	1.4959527	-0.4534234
H	4.6073772	2.1447517	1.4921246
H	3.4416082	0.0399967	2.0044576
H	4.6399322	-1.5363123	-1.8430814
H	5.7975362	0.5776477	-2.3354334
H	5.7898272	2.4255867	-0.6749774
C	3.2790042	-2.1424403	0.4150526
C	3.2644222	-3.2247253	-0.4935934
N	3.2521122	-4.1144593	-1.2371974
C	2.5975282	-2.3491663	1.6357986
N	2.0384882	-2.5210243	2.6371386

XIII. References

(1) Hamilton, D. S.; Nicewicz, D. A. *J. Am. Chem. Soc.* **2012**, *134*, 18577–18580.
(2) Wilger, D. J.; Gesmundo, N. J.; Nicewicz, D. A. *Chem. Sci.* **2013**, *4*, 3160–3165.
(3) Kuruvilla, E.; Ramaiah, D. *J. Phys. Chem. B* **2007**, *111*, 6549–6556.
(4) Seiders, J. R.; Wang, L.; Floreancig, P. E. *J. Am. Chem. Soc.* **2003**, *125*, 2406–2407.
(5) Horn, M.; Schappele, L. H.; Lang-Wittkowski, G.; Mayr, H.; Ofial, A. R. *Chem. – Eur. J.* **2013**, *19*, 249–263.
(6) Weber, G.; Teale, F. W. J. *Trans Faraday Soc* **1957**, *53*, 646–655.
(7) Benniston, A. C.; Harriman, A.; Li, P.; Rostron, J. P.; van Ramesdonk, H. J.; Groeneveld, M. M.; Zhang, H.; Verhoeven, J. W. *J. Am. Chem. Soc.* **2005**, *127*, 16054–16064.
(8) Knauf, R. R.; Brennaman, M. K.; Alibabaei, L.; Norris, M. R.; Dempsey, J. L. *J. Phys. Chem. C* **2013**, *117*, 25259–25268.
(9) Fukuzumi, S.; Kotani, H.; Ohkubo, K.; Ogo, S.; Tkachenko, N. V.; Lemmetyinen, H. *J. Am. Chem. Soc.* **2004**, *126*, 1600–1601.
(10) Fukuzumi, S.; Kotani, H.; Ohkubo, K. *Phys. Chem. Chem. Phys.* **2008**, *10*, 5159.
(11) Koelle, U.; Infelta, P. P.; Graetzel, M. *Inorg. Chem.* **1988**, *27*, 879–883.
(12) Sattler, W.; Ener, M. E.; Blakemore, J. D.; Rachford, A. A.; LaBeaume, P. J.; Thackeray, J. W.; Cameron, J. F.; Winkler, J. R.; Gray, H. B. *J. Am. Chem. Soc.* **2013**, *135*, 10614–10617.
(13) Riyad, Y. M.; Naumov, S.; Hermann, R.; Brede, O. *Phys. Chem. Chem. Phys.* **2006**, *8*, 1697.
(14) Benesi, H. A.; Hildebrand, J. H. *J. Am. Chem. Soc.* **1949**, *71*, 2703–2707.
(15) Foster, R. *Organic Charge-Transfer Complexes*; Academic Press Inc. Ltd.: London, 1969.
(16) Nash, C. P. *J. Phys. Chem.* **1960**, *64*, 950–953.
(17) Johnson, R. C. *J. Chem. Educ.* **1970**, *47*, 702.
(18) Kirk, A. D.; Namasivayam, C. *Anal. Chem.* **1983**, *55*, 2428–2429.
(19) Demas, J. N.; Bowman, W. D.; Zalewski, E. F.; Velapoldi, R. A. *J. Phys. Chem.* **1981**, *85*, 2766–2771.
(20) *Gaussian 09, Revision D.01,* M. J. Frisch, G. W. Trucks, H. B. Schlegel, G. E. Scuseria, M. A. Robb, J. R. Cheeseman, G. Scalmani, V. Barone, B. Mennucci, G. A. Petersson, H. Nakatsuji, M. Caricato, X. Li, H. P. Hratchian, A. F. Izmaylov, J. Bloino, G. Zheng, J. L. Sonnenberg, M. Hada, M. Ehara, K. Toyota, R. Fukuda, J. Hasegawa, M. Ishida, T. Nakajima, Y. Honda, O. Kitao, H. Nakai, T. Vreven, J. A. Montgomery, Jr., J. E. Peralta, F. Ogliaro, M. Bearpark, J. J. Heyd, E. Brothers, K. N. Kudin, V. N. Staroverov, R. Kobayashi, J. Normand, K. Raghavachari, A. Rendell, J. C. Burant, S. S. Iyengar, J. Tomasi, M. Cossi, N. Rega, J. M. Millam, M. Klene, J. E. Knox, J. B. Cross, V. Bakken, C. Adamo, J. Jaramillo, R. Gomperts, R. E. Stratmann, O. Yazyev, A. J. Austin, R. Cammi, C. Pomelli, J. W. Ochterski, R. L. Martin, K. Morokuma, V. G. Zakrzewski, G. A. Voth, P. Salvador, J. J. Dannenberg, S. Dapprich, A. D. Daniels, Ö. Farkas, J. B. Foresman, J. V. Ortiz, J. Cioslowski, and D. J. Fox, Gaussian, Inc., Wallingford CT, 2009.
(21) Becke, A. D. *J. Chem. Phys.* **1993**, *98*, 5648–5652.
(22) Lee, C.; Yang, W.; Parr, R. G. *Phys. Rev. B* **1988**, *37*, 785–789.
(23) Krishnan, R.; Binkley, J. S.; Seeger, R.; Pople, J. A. *J. Chem. Phys.* **1980**, *72*, 650–654.
(24) McLean, A. D.; Chandler, G. S. *J. Chem. Phys.* **1980**, *72*, 5639–5648.
(25) Tomasi, J.; Mennucci, B.; Cammi, R. *Chem. Rev.* **2005**, *105*, 2999–3094.
(26) Legault, C. Y. *CYLview, 1.0b;* Université de Sherbrooke, 2009 (http://www.cylview.org).